Mapping T cell activation and differentiation at single cell resolution in naive hosts infected with *Plasmodium vivax*

Florian A. Bach,[1*] Diana Muñoz Sandoval,[1,2] Michalina Mazurczyk,[3] Yrene Themistocleous,[4] Thomas A. Rawlinson,[4] Alison Kemp,[5] Sarah E. Silk,[4] Jordan R. Barrett,[4] Nick J. Edwards,[4] Alasdair Ivens,[1,6] Julian C. Rayner,[5,7] Angela M. Minassian,[4] Giorgio Napolitani,[3] Simon J. Draper,[4] and Philip J. Spence[1,6*]

[1]Institute of Immunology and Infection Research, University of Edinburgh, Edinburgh, UK. [2]Instituto de Microbiologia, Universidad San Francisco de Quito, Quito, Ecuador. [3]MRC Human Immunology Unit, Weatherall Institute of Molecular Medicine, University of Oxford, Oxford, UK. [4]The Jenner Institute, University of Oxford, Oxford, UK. [5]Wellcome Sanger Institute, Cambridge, UK. [6]Centre for Immunity, Infection and Evolution, University of Edinburgh, Edinburgh, UK. [7]Cambridge Institute for Medical Research, School of Clinical Medicine, University of Cambridge, Cambridge, UK.

[*]correspondence: florian.bach@ed.ac.uk and philip.spence@ed.ac.uk

The biology of *Plasmodium vivax* is markedly different to that of *P. falciparum*; how this shapes the immune response to infection remains unclear. To address this shortfall, we inoculated human volunteers with a clonal field isolate of *P. vivax* and tracked their response through infection and convalescence. High dimensional protein and RNA-seq data show that *P. vivax* triggers an acute phase response that shares remarkable overlap with that of *P. falciparum*, suggesting a hardwired emergency myeloid response that does not discriminate parasite species. We then used cytometry by time of flight to analyse the fate and function of innate-like and adaptive T cells; these data show that *P. vivax* can activate up to one quarter of the entire T cell compartment. Heterogeneous effector memory-like $CD4^+$ T cells dominate this extraordinary response and phenotypic analysis reveals unexpected features of terminal differentiation that are normally associated with cytotoxicity and autoinflammatory disease. In line with this observation, we found that $CD4^+$ T cell activation coincides with collateral tissue damage and liver injury. Finally, comparative analyses demonstrate that *P. falciparum* drives T cell activation far in excess of *P. vivax*, which may partially explain why falciparum malaria more frequently causes severe disease.

Introduction

Plasmodium vivax causes more than half of all malaria cases in the Americas and South-East Asia; globally, around 14 million annual cases present a significant clinical and economic burden (1). Whilst efficacious drugs are available to clear the blood-stage of infection the dormant liver stage of *P. vivax* (the hypnozoite) can persist and cause multiple relapses over many months and years. All available hypnozoitocidal drugs can cause haemolysis in patients with glucose-6-phosphate dehydrogenase (G6PD) deficiency, a highly prevalent polymorphism in many endemic populations (2, 3). This poses a unique challenge for the elimination of *P. vivax*, and forces public health services to balance the risk of potentially severe adverse treatment events (4) with the benefit of reducing malaria burden (3, 5). A vaccine that blocks parasite transmission or reduces the frequency or severity of clinical episodes would be an important step towards control and elimination, and yet vaccine development for *P. vivax* lags behind the far better studied *P. falciparum* (6). What's more, there are large gaps in understanding the immune response to *P. vivax* and the consequences for pathology versus protection; this inevitably leads to assumptions based on the findings from falciparum malaria rather than direct experimental evidence. However, the distinct biology, pathology and epidemiology of *P. vivax* suggests that these parasites do not interact with the human immune system in the same way as *P. falciparum*. Consequently, the immune response could have an important role in shaping the discrete outcomes of vivax and falciparum malaria.

Plasmodium vivax is evolutionarily divergent from *Plasmodium falciparum* (7) and its genome is significantly less AT-rich. CpG islands are therefore more prevalent in *P. vivax* (8) and these DNA motifs can trigger TLR9 signalling and inflammation (9), which may partially explain why it has a much-reduced pyrogenic threshold compared to *P. falciparum* (10). Furthermore, *P. vivax* preferentially invades $CD71^+$ reticulocytes (11, 12), which express class I MHC and high levels of CD47 in contrast to mature red cells (the target cell for *P. falciparum*). This provides a unique route to pathogen control in vivax malaria - the direct cytolysis of infected reticulocytes by antigen-specific $CD8^+$ T cells (13). A hallmark of *P. falciparum* infected red cells is their increased rigidity, which makes them vulnerable to mechanical trapping and clearance in the spleen; in contrast, *P. vivax* infected reticulocytes become more deformable allowing for rapid egress from this site of immune surveillance (14). Importantly, *P. vivax* shows reduced cytoadherance to the endothelium and therefore sequesters less effectively than *P. falciparum*. Tissue distribution patterns are also distinct with *P. vivax* more commonly accumulating in high numbers in the bone marrow (15) and lung (16). But perhaps the most significant difference is that severe disease is a much more common outcome of falciparum malaria (17) and clinical immunity (leading to asymptomatic infection) is acquired much more quickly with *P. vivax* (18, 19). This observation was also made during the malariotherapy era, which demonstrated under controlled settings that a single episode of vivax malaria was sufficient to reduce the incidence of fever in subsequent infections (20-22).

The myriad ways in which *P. vivax* differs from *P. falciparum* therefore necessitates experimental systems and tools that are tailored specifically towards vivax malaria. This is made harder by the absence of long-term culture-adapted parasites and a consequence of

this shortfall has been a resurgence in the use of human challenge models (23). Controlled human malaria infection (CHMI) was re-established for *P. falciparum* in 1986 but only very recently for *P. vivax* (24-27). To harness the exciting potential of this development we generated a new cryopreserved stabilate of *Plasmodium vivax* suitable for CHMI and used a hybrid PacBio/Illumina assembly technique to generate a reference quality parasite genome (see the accompanying article by Minassian *et al.*). Here we use systems immunology tools (including cytometry by time of flight (CyTOF)) to map the host response to *P. vivax* at unprecedented resolution. In the first instance, we tracked the acute phase response to ask how blood-stage parasites activate the innate immune system; we then examined the relationship between systemic inflammation and T cell activation. Human T cells are uniquely placed to influence the outcome of infection as they enter inflamed tissues, regulate myeloid cell activation, promote humoral immunity and even kill *Plasmodium* infected red cells (13, 28). What's more, T cells can directly cause collateral tissue damage and pathology (29-31). Mapping the heterogeneity of T cell activation and differentiation was therefore a priority for this study. Finally, we reasoned that a comparison between the host response to *P. vivax* and *P. falciparum* may shed new light on why falciparum malaria more frequently causes severe disease and why *Plasmodium vivax* is better able to induce rapid clinical immunity.

91 # Results

92 ### ***Plasmodium vivax*** **triggers interferon-stimulated inflammation**

93 Six volunteers were recruited into a clinical trial (VAC069A) to assess the infectivity of a new
94 cryopreserved *P. vivax* stabilate, which we have called PvW1 (supplementary file 1).
95 Importantly, these parasites originated from a naturally-infected donor in Thailand with a
96 single genotype infection and were mosquito-transmitted prior to cryopreservation (see
97 Minassian *et al.* for details). Each volunteer was successfully infected by direct blood
98 challenge and reached the parasitaemic threshold necessitating treatment (5,000 or 10,000
99 parasite genomes ml^{-1} in the presence or absence of symptoms, respectively) within 12-16
100 days of inoculation (figure 1A). Whole blood samples were taken at baseline (day before
101 challenge), during infection (e.g. C7 for 7-days post-challenge), immediately before
102 treatment (termed diagnosis), soon after treatment (e.g. T6 for 6-days post-treatment) and
103 45-days after challenge (memory phase).

104 The total number of recorded adverse events (including symptomatology, haematology and
105 blood chemistry) peaked within 24-hours of treatment and largely resolved by T6. All
106 volunteers exhibited pronounced lymphopenia (an adverse event in 5/6 volunteers) and
107 pyrexia (4/6) and thrombocytopenia (3/6) were also common features of infection (figure 1B
108 and Minassian *et al.*). All adverse events were self-limiting and did not require specific
109 interventions. Notably, alanine aminotransferase (ALT) increased in plasma six days post-
110 treatment and was an adverse event in 4/6 volunteers (figure 1C). This can be indicative of
111 hepatocellular death and liver injury - a reversible phenomenon in uncomplicated malaria
112 (32-34) - and occurred at the same time that lymphocyte counts returned to baseline. Taken
113 together, these results show that volunteers infected with *Plasmodium vivax* (clone PvW1)
114 develop hallmark signs and symptoms of clinical malaria.

115 Next, we sought to capture the acute phase response to *P. vivax* by quantifying 39 plasma
116 analytes including cytokines, chemokines and biomarkers of coagulation and oxidative
117 stress using a custom bead-based array. Platelet-free plasma samples collected at baseline,
118 diagnosis, T6 and 45-days post-challenge were used to create a time-course of abundance
119 for each analyte. To identify analytes that varied significantly through time we fitted linear
120 models for each analyte in the form of analyte~timepoint+volunteer using log10 transformed
121 concentrations and time-point as a categorical variable. After correcting for multiple testing,
122 we found 12 analytes with an FDR < 0.05 (figure 1D).

123 All significant analytes were found to increase in abundance and all peaked at diagnosis with
124 the exception of IL-18, which was significantly elevated at T6. The analyte with the lowest
125 FDR was IFNγ indicating a type I inflammatory response, which has been extensively
126 described in falciparum malaria (35). Key functional consequences of this response include
127 recruitment of monocytes (CCL2) and T cells (CXCL9, CXCL10), as well as their activation
128 and differentiation (IL-12, IL-18, IL-21). Inflammation is intimately linked to coagulation and
129 D-Dimer (a fibrin degradation product indicative of intravascular fibrinolysis) was found to be
130 significantly increased in all volunteers. This is a known feature of clinical malaria (36) that
131 has been linked to disease severity (37, 38). In conclusion, *Plasmodium vivax* triggers an
132 interferon-induced type I inflammatory response that coincides with hallmark features of

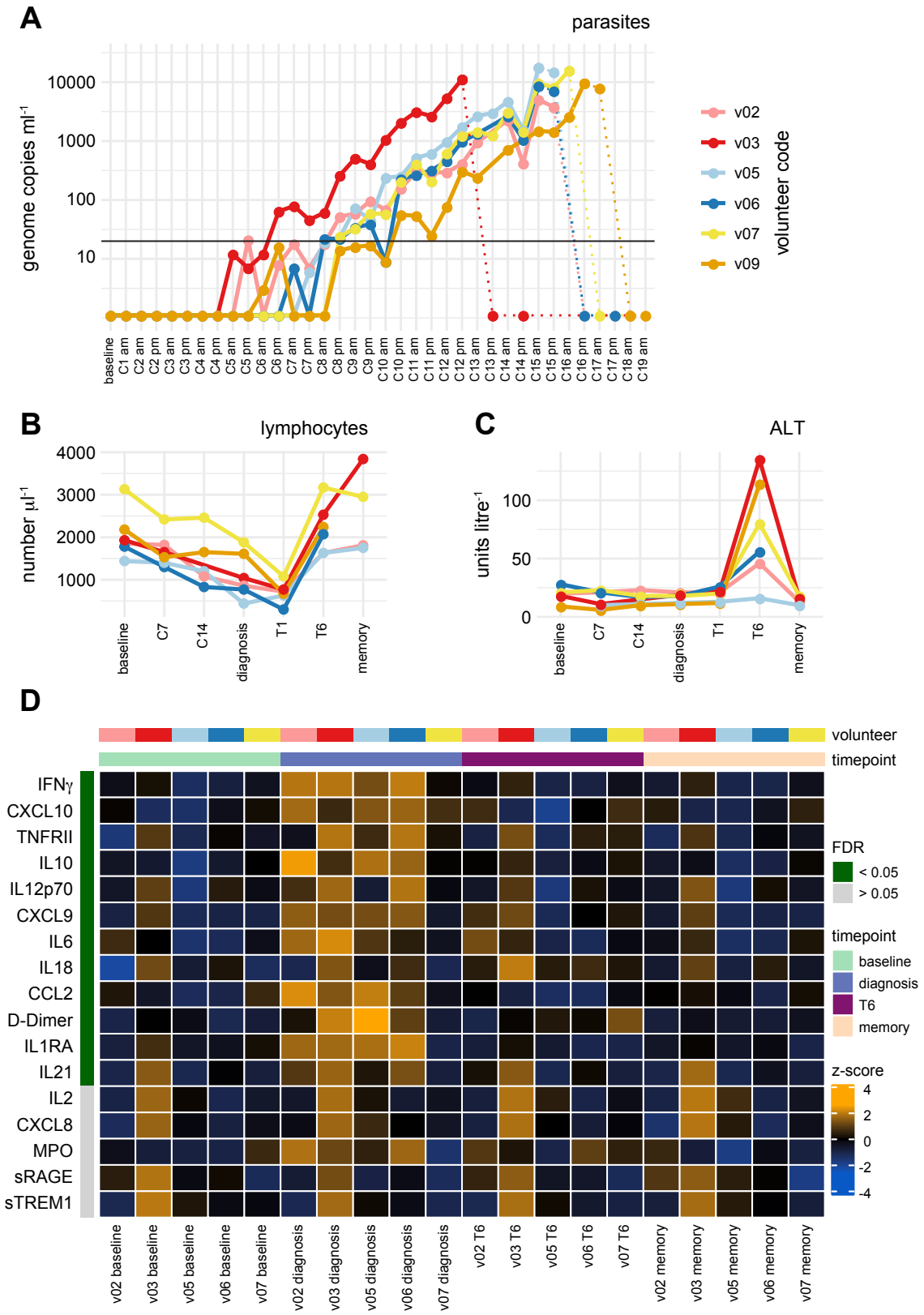

Figure 1 | *Plasmodium vivax* triggers interferon-stimulated inflammation. (**A**) Parasitaemia was determined twice daily by qPCR. Pre-treatment measurements are shown as solid lines, post-treatment measurements as dotted lines. The limit of quantification (20 genome copies ml^{-1}) is shown by a black line. (**B**-**C**) Full blood counts and blood chemistry measured (B) lymphocyte frequencies and (C) the concentration of alanine aminotransferase (ALT) throughout infection and convalescence. (**D**) Multiplexed plasma analytes were measured using a custom Legendplex assay. Each row in the heatmap is an analyte and each column a plasma sample. Samples from v09 were excluded after failing QC. Linear modelling was used to identify analytes that varied significantly through time across the cohort, and these are ordered by FDR. Only 17 of the 39 analytes measured are shown in the heatmap (those with the lowest FDR); the colour of each tile corresponds to the row-wise z-score transformed concentrations. In (B and C) the memory time-point is 90-days post-challenge and in (D) memory is 45-days post-challenge.

133 clinical disease, including lymphopenia, pyrexia and fibrinolysis. Importantly, clinical
134 presentation and plasma analytes largely return to baseline levels within six days of drug
135 treatment with the exception of IL-18 and ALT, which are induced post-treatment and peak
136 at T6.

137 **Interferon signalling is followed by a signature of cell proliferation in whole blood**

138 To further characterise the systemic response to *P. vivax* we used bulk RNA-sequencing to
139 resolve changes in whole blood gene expression through time. Samples were collected at
140 baseline, throughout infection, diagnosis and T6 giving a time-course of 7-9 samples per
141 volunteer. DESeq2 (39) was then used for pairwise comparisons to resolve conserved
142 responses between volunteers; samples were thus grouped by time-point and compared to
143 baseline. Differential gene expression was defined as an adjusted p value < 0.05 and an
144 absolute fold change > 1.5 - the transcriptional response peaked at diagnosis with 2221
145 differentially expressed genes (DEG). Of note, no DEG were found as late as C12, which
146 implies that the transcriptional response at diagnosis was rapidly induced. This may indicate
147 that parasite density (rather than time elapsed) is the primary trigger for systemic
148 inflammation in a naive host. Surprisingly, only 298 DEG were found at T6 and most of these
149 genes (66%) were unique to this time-point, which shows that a distinct transcriptional
150 response follows drug treatment.

151 To infer biological function of the host response at diagnosis and T6 we used gene ontology
152 (GO) network analysis using ClueGO (40, 41). First, all DEG from diagnosis and T6 were
153 combined to identify significantly enriched GO terms. Then a graph-based non-redundant
154 network was constructed with each GO term placed as a node and with edges connecting
155 nodes that shared associated genes. Finally, GO terms were placed into groups that have
156 significant inter-connectivity, meaning a highly related biological function of each node within
157 a group. Critically, for each GO term information on what fraction of associated genes are
158 differentially expressed at diagnosis or T6 is retained; this allows for a direct comparison of
159 the transcriptional response between time-points at a functional level. This analysis revealed
160 diverging and disconnected biological functions at diagnosis and T6 (figure 2).

161 The transcriptional response at diagnosis is dominated by upregulation of innate signalling
162 and defence pathways, including GO terms associated with NF-κB signalling, activation of
163 myeloid cells, leukocyte migration and cytokine production. These pathways and functional
164 groups were also identified when we and others analysed the transcriptional response to *P.*
165 *falciparum* in naive hosts (35, 42, 43) and this signature is consistent with interferon-
166 stimulated systemic inflammation. As volunteers are lymphopenic at this time-point the
167 majority of these transcriptional changes are likely to derive from myeloid cells, which are
168 initially activated by malaria parasites in the bone marrow (44). The changes we capture in
169 whole blood during infection may therefore reveal the trafficking of activated monocytes and
170 neutrophils as they transit from the bone marrow to inflamed tissues, such as the spleen. On
171 the other hand, the GO terms unique to T6 all relate to cell cycle progression and nuclear
172 division, rather than inflammation. This signature is unlikely to derive from activated myeloid
173 cells, as in general they are terminally differentiated and do not proliferate in the circulation.

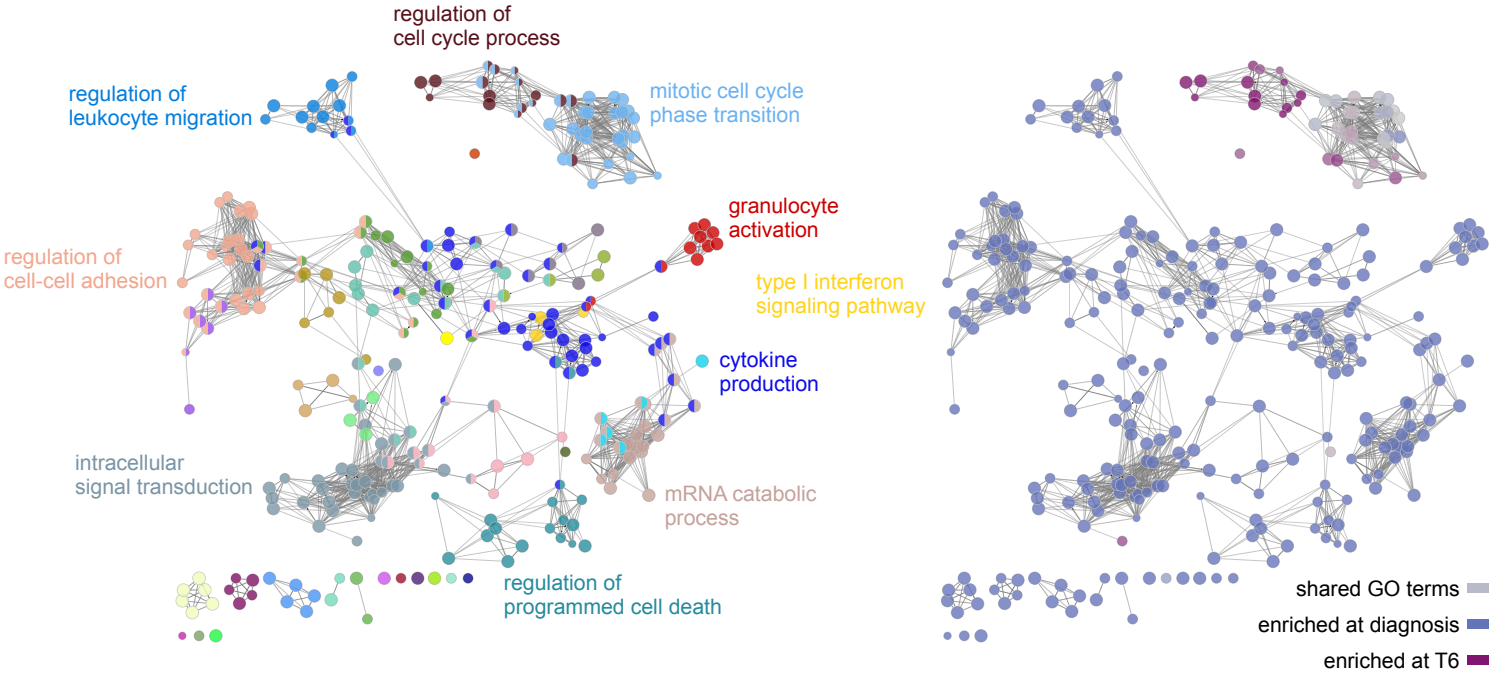

Figure 2 | Interferon signalling is followed by a signature of cell proliferation in whole blood. Differentially expressed genes at diagnosis and T6 were combined for GO analysis. GO terms (nodes) that share associated genes are connected by an edge and edges pull GO terms into groups according to interconnectivity and overlapping function. In the left panel, each node is coloured according to functional group (named by choosing a representative GO term for each group). In the right panel, the same network is now coloured according to whether a clear majority (> 65%) of associated genes were differentially expressed at diagnosis (blue) or T6 (purple).

174 Instead, these data suggest that we are capturing activated lymphocytes as they return to
175 the circulation after parasite clearance.

176 In summary, *P. vivax* induces two distinct transcriptional programmes in whole blood during
177 and after infection. During infection, transcriptional profiling reveals the rapid mobilisation of
178 an emergency myeloid response, consistent with observations in falciparum malaria. Six
179 days after treatment, this innate response subsides and a transcriptional signature of
180 proliferation is revealed, which indicates widespread activation of lymphocytes.

181 ***Plasmodium vivax* triggers global activation of innate-like and adaptive T cells**

182 It is well known that T cells are recruited out of the circulation during infection and activated
183 within the inflamed spleen (45); by studying their phenotype as they re-enter the circulation
184 at T6 it may be possible to measure T cell priming and the tissue environment in human
185 malaria. To explore this idea further we leveraged cytometry by time of flight (CyTOF) to
186 achieve single cell resolution of T cell activation and differentiation. Whole blood samples
187 were preserved within 30-minutes of blood draw to create a detailed time-series of the T cell
188 compartment and data from all volunteers were concatenated to identify conserved changes
189 through time. To examine these data we first used Uniform Manifold Approximation and
190 Projection (UMAP (46)) to visualise the phenotypic diversity of T cells at each time-point.
191 Cells close to each other in the UMAP space are phenotypically similar, whereas dissimilar
192 cells are far apart. Remarkably, the global structure of the T cell compartment appears
193 stable between baseline and diagnosis (figure 3A) despite pronounced lymphopenia as
194 infection progresses. At T6 however, a dense population of T cells appears *de novo* and
195 inspection of key markers associated with lineage and memory (supplementary figure 1)
196 indicates that these are predominantly $CD4^+$ T cells with an effector memory ($CD45RA^-$
197 $CD45RO^+CCR7^-$) and activated phenotype ($CD38^{hi}Bcl2^{lo}$) (figure 3B-C). Using the latter
198 marker combination to identify activated T cells across all lineages, we found a surprisingly
199 large fraction of the T cell compartment activated at T6 (up to 22% of all T cells) including
200 innate-like gamma delta T cells and MAIT cells (figure 3D-E).

201 In order to more comprehensively describe phenotypic changes in T cells we used FlowSOM
202 clustering (47) and manual merging to assign each T cell to one of 34 non-overlapping
203 clusters (supplementary figure 2). Tracking the frequency of each cluster through time then
204 resolved the dynamic changes in the T cell compartment as a consequence of infection
205 (supplementary figure 3). To statistically determine which clusters vary significantly through
206 time we performed linear regression on cell count data using *edgeR* (48, 49). In this way, we
207 could identify differentially abundant clusters at each time-point relative to baseline. We
208 found no clusters differentially abundant at C10 and only one cluster ($CD161^+$ gamma delta)
209 downregulated at diagnosis (FDR < 0.05 and absolute fold change > 2). That only one of 34
210 clusters significantly changed in their relative size as the host became lymphopenic indicates
211 that T cells are proportionally recruited out of the circulation regardless of lineage, function or
212 memory, suggesting a relatively indiscriminate mechanism of recruitment.

213 Using the same significance cut-offs we identified nine clusters that increased in abundance
214 at T6 (figure 4A-B) - these clusters were comprised of five $CD4^+$ and two $CD8^+$ T cell

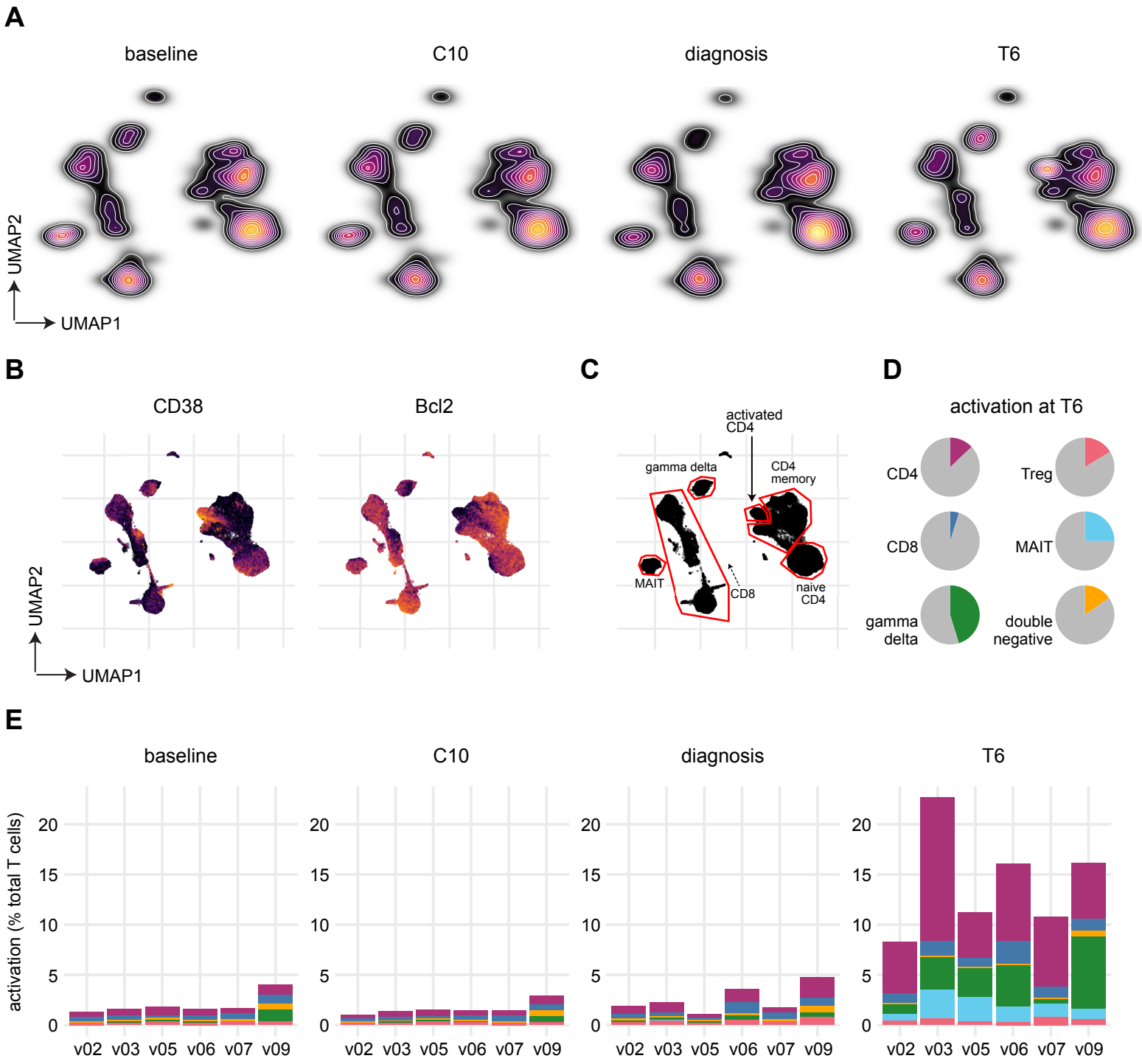

Figure 3 | *Plasmodium vivax* triggers global activation of innate-like and adaptive T cells. Whole blood was preserved within 30-minutes of blood draw at baseline, C10, diagnosis and T6. Samples were stained with a T cell focussed antibody panel (details in supplementary file 2) and acquired on a Helios mass cytometer. (**A**) UMAP projection coloured by cell density and split by time-point. (**B**) Expression of CD38 and Bcl2 across the UMAP projection at T6; each marker is independently scaled using arcsine transformed signal intensity. (**C**) UMAP projection with gates and labels indicating the location of each major T cell subset (shown at T6, see supplementary file 1 for the expression of lineage and memory markers). Note that the dashed arrow indicates the direction of terminal differentiation for $CD8^+$ T cells (e.g. TEMRA are adjacent to gamma delta T cells) (**D**) Mean proportion of each T cell subset that is activated ($CD38^{hi}$ $Bcl2^{lo}$) at T6. (**E**) Stacked bar chart showing the frequency of activated T cells at each time-point; bars are colour-coded by lineage as in (D).

215 subsets, plus one MAIT and one gamma delta subset. Critically, all displayed a CD38^{hi}Bcl2^{lo}
216 phenotype (figure 3B and figure 4A) statistically confirming widespread activation of all T
217 lineages. Notably, although a cluster of activated regulatory T cells increased in abundance
218 at T6 this did not reach statistical significance, most likely due to our small sample size.
219 Collectively, these results suggest that innate-like and adaptive T cells are indiscriminately
220 recruited out of circulation and activated by *P. vivax*. The breadth and scale of T cell
221 activation considerably exceeds what has been observed in other human challenge models,
222 including typhoidal *Salmonella* (50) and influenza A (51).

223 **Heterogeneous effector memory-like CD4$^+$ T cells dominate the adaptive response**

224 In order to elucidate the function of activated T cells as they re-enter the circulation we
225 inspected the median expression values of proliferation and differentiation markers in the
226 nine T cell clusters that increased in abundance at T6 (figure 5A and supplementary figure
227 4). And because we found more than half of all activated T cells were CD4$^+$ (with five distinct
228 clusters contained within this lineage (figure 5B)) we examined in detail the heterogeneity of
229 the CD4$^+$ T cell response. High CD38 expression and low Bcl2 expression was a shared
230 feature of all significant clusters and 4/5 displayed an effector memory phenotype (CD45RA$^-$
231 CD45RO$^+$CCR7$^-$). The one exception was a small cluster of activated central memory-like
232 CD4$^+$ T cells (CD45RA$^-$CD45RO$^+$CCR7$^+$). By summing these five CD45RO$^+$ clusters we
233 found that *P. vivax* activates 20-35% of the non-naive CD4$^+$ T cell pool (figure 5C).

234 The T cell activation markers HLA-DR and ICOS were a common (but not ubiquitous)
235 feature of activated CD4$^+$ T cells and we also found widespread expression of inhibitory
236 receptors, such as PD1 and CTLA4 (figure 5D). These checkpoint inhibitors are often used
237 to identify exhausted T cells and yet our volunteers experienced a relatively short and acute
238 infection (rather than chronic stimulation). However, it is now recognised that upregulation of
239 these receptors can also act to self-regulate short-lived responses (52, 53). In agreement,
240 we found that many activated CD4$^+$ T cells were CD28^{hi}, T-bet$^+$ and proliferative (Ki-67$^+$)
241 indicating polarisation towards a functional and inflammatory T_H1 fate (figure 5A).

242 Perhaps surprisingly, the largest cluster of activated CD4$^+$ T cells had a CD27$^-$ cytotoxic
243 phenotype (perforin$^+$ granzyme B$^+$) (figure 5A, B and D). Loss of CD27 expression and gain
244 of cytotoxic functions is not a common outcome of CD4$^+$ T cell activation in human infectious
245 disease. Rather, this phenotype usually arises in contexts of persistent antigen stimulation
246 (54) or in conditions associated with collateral tissue damage, such as pulmonary
247 tuberculosis (55), IgG4-related disease (56) or rheumatoid arthritis (57). Whether this
248 phenotype is specific to *Plasmodium vivax* or is a shared feature with *P. falciparum* remains
249 to be seen. In summary, CD4$^+$ T cells with an effector memory phenotype dominate the
250 adaptive response to *P. vivax* and display marked heterogeneity in their expression of key
251 markers of T cell function and fate (figure 5D). These data therefore emphasise the
252 complexity of CD4$^+$ T cell activation and differentiation in vivax malaria.

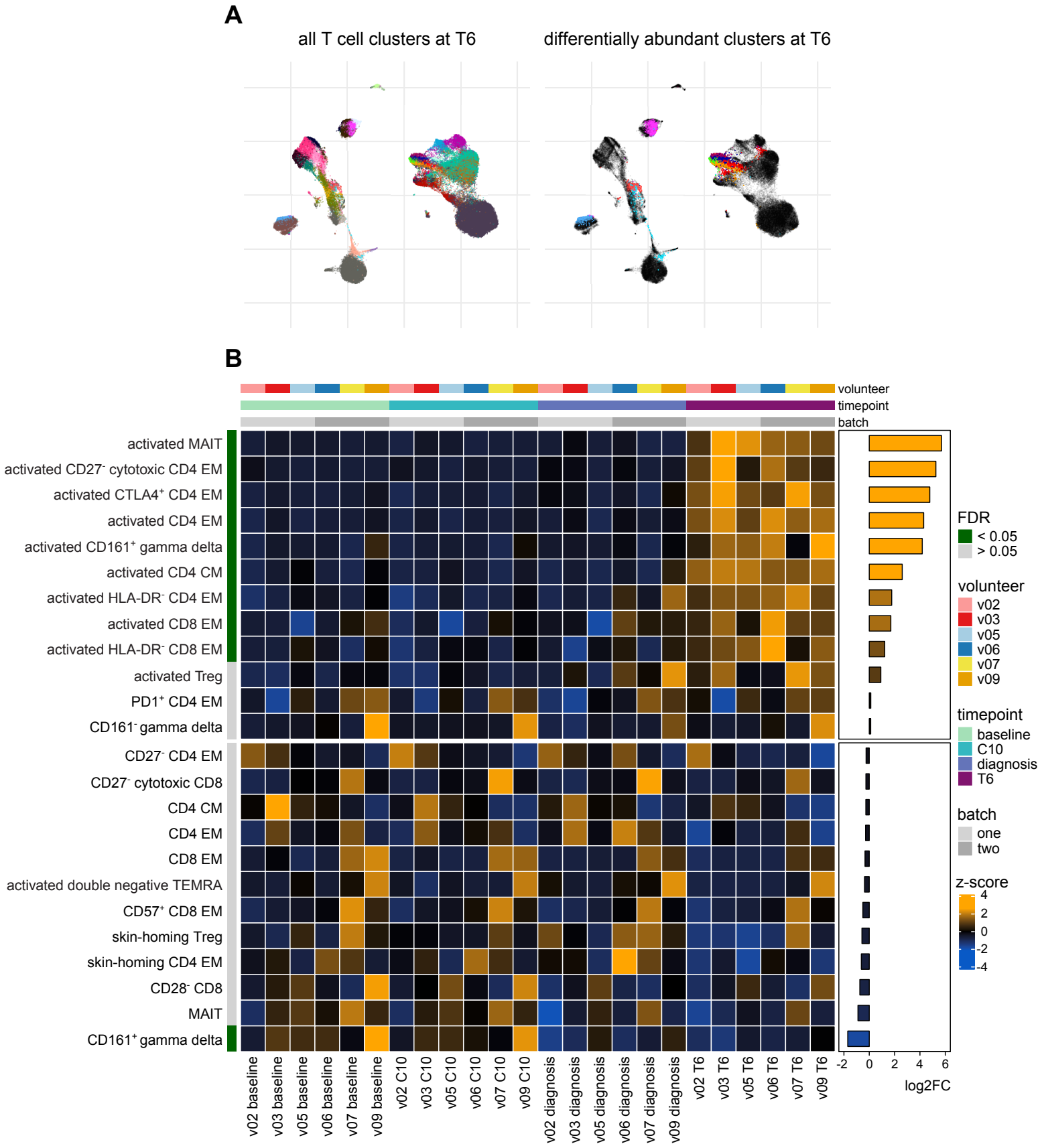

Figure 4 | Differential abundance of T cell clusters through time. (**A**) UMAP projection showing all 34 T cell clusters (left) and those that were differentially abundant at T6 (right). Each cluster has a unique colour. (**B**) Heatmap showing the relative abundance of T cell clusters through time. Each row is a T cell cluster and each column a sample; clusters are ordered by log2 fold change at T6 (relative to baseline). Only 24 of the 34 T cell clusters are shown (those with the lowest FDR) and tiles are coloured according to row-wise (arcsine square root transformed) frequency z-scores.

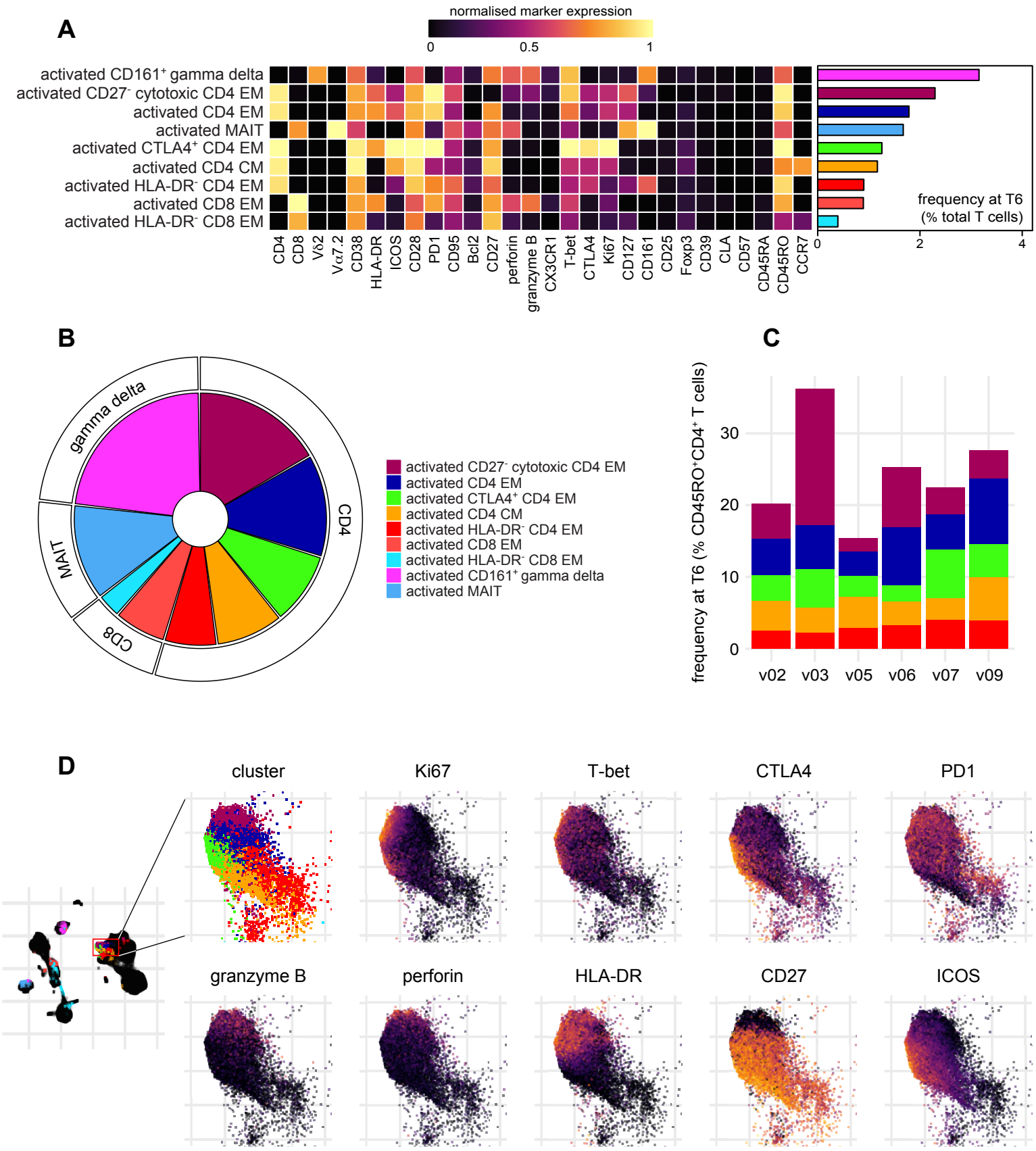

Figure 5 | Heterogeneous effector memory-like CD4⁺ T cells dominate the adaptive response. (**A**) Heatmap showing normalised median expression values of all markers used for clustering in each of the 9 T cell clusters that were differentially abundant at T6; the horizontal bar chart shows the average frequency of each cluster across all volunteers. (**B**) Pie showing the relative size of each differentially abundant T cell cluster. (**C**) Stacked bar chart showing each differentially abundant CD4⁺ T cell cluster as a proportion of the total non-naive (CD45RO⁺) CD4⁺ T cell pool. (**D**) UMAP projection showing the expression of activation, proliferation and differentiation markers across each of the differentially abundant CD4⁺ T cell clusters at T6; each marker is independently scaled using arcsine transformed signal intensity.

253 **T cell activation occurs independently of systemic inflammation**

254 Innate-like and adaptive T cells have distinct ligand requirements for TCR signalling and yet
255 every major T cell subset is activated by *P. vivax* (figure 4A-B). We therefore hypothesised
256 that the scale and breadth of the T cell response may indicate bystander (antigen-
257 independent) activation, which can be caused by systemic inflammation (58-61). To
258 investigate the relationship between the interferon-induced type I inflammatory response
259 observed at diagnosis and T cell activation at T6 we constructed a Pearson correlation
260 matrix (figure 6A). We input the log2 fold change of each plasma analyte with an FDR < 0.05
261 and the log2 fold change of each activated T cell cluster (defined as $CD38^{hi}Bcl2^{lo}$). To
262 examine all possible correlations we chose to include all activated T cell clusters regardless
263 of whether their abundance was significantly increased or not. Fold change was calculated
264 for each feature at either diagnosis or T6 (relative to baseline) depending on when the peak
265 response was observed. Hierarchical clustering on the matrix revealed extensive positive
266 correlation between inflammatory cytokines, chemokines and coagulation at diagnosis. In
267 contrast, only one T cell cluster correlated highly with these analytes (r > 0.8 for activated
268 CD8 effector memory) and just two clusters showed weak correlations (activated $CD161^{+}$
269 gamma delta and activated CD4 effector memory). Instead, the majority of T cell clusters
270 (8/11) were placed into a separate clade together with ALT, which indicates that the majority
271 of the T cell response is co-regulated but operates independently of systemic inflammation.

272 We next looked at the co-regulation of T cell activation and ALT in more detail. Elevations in
273 plasma ALT showed a highly positive correlation with expansion of activated Tregs (r = 0.97)
274 and a modest positive correlation with four activated $CD4^{+}$ T cell clusters, indicating a
275 possible association between T cell activation and collateral tissue damage. Because this
276 analysis was looking for independent relationships between each T cell cluster and ALT we
277 decided to repeat this analysis at a subset level. To this end, we calculated the correlation
278 between lineage-specific T cell activation and absolute ALT levels at T6 and found a
279 significant or near significant association with activated $CD4^{+}$ T cells (r = 0.791, p = 0.061)
280 and regulatory T cells (r = 0.816, p=0.0478) but not innate-like MAIT (r = 0.147, p= 0.781) or
281 gamma delta T cells (r = 0.107, p = 0.841) (figure 6B). In summary, there is no clear
282 relationship between the intensity of systemic inflammation at diagnosis and the magnitude
283 of the T cell response at T6. In contrast, activation of $CD4^{+}$ and regulatory T cells positively
284 correlates with elevations in circulating ALT, which suggests that the adaptive T cell
285 response to *P. vivax* may be an accurate indicator of collateral tissue damage.

286 **Parasite species regulates $CD4^{+}$ T cell activation**

287 Last of all, we wanted to investigate whether the immune response to *P. vivax* differed from
288 that to the far better studied pathogen *P. falciparum*. Initially, we compared transcriptional
289 signatures in whole blood between volunteers infected with *P. vivax* (this study) and *P.*
290 *falciparum* (a CHMI trial we conducted previously with time-matched samples (VAC063C)).
291 Importantly, volunteers in both studies were malaria-naive, infected by blood challenge and
292 diagnosed and drug treated at the same parasite density (see methods). Differentially
293 expressed genes (adj p < 0.05 and absolute fold change > 1.5) were identified at diagnosis
294 and T6 (relative to baseline) in both volunteer cohorts using DESeq2. The DEG from each

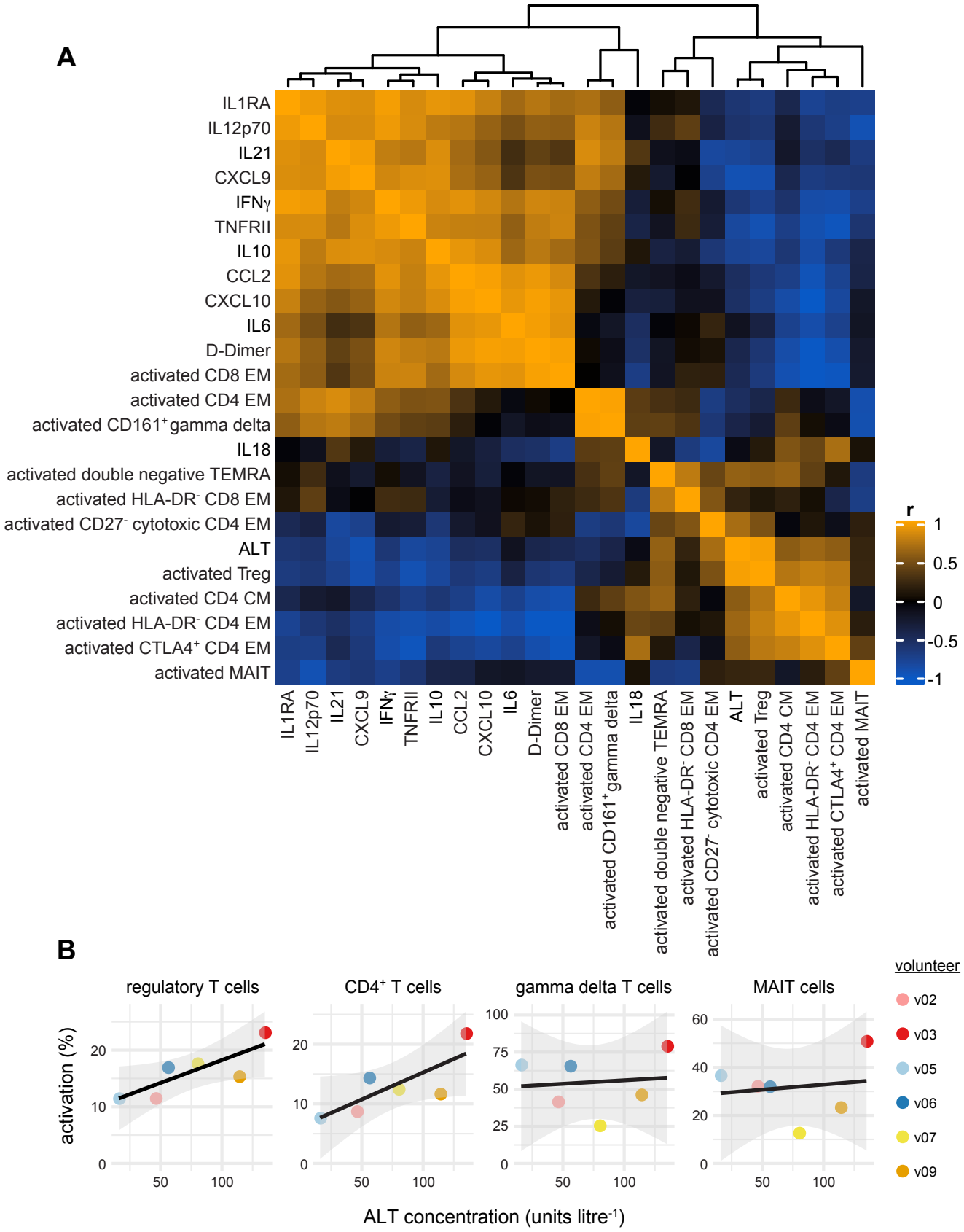

Figure 6 | T cell activation occurs independently of systemic inflammation. (**A**) Heatmap showing a Pearson correlation matrix of the log2 transformed fold change of each activated T cell cluster and the twelve most variable plasma analytes (FDR < 0.05). Fold change was calculated either at diagnosis or T6 (relative to baseline) according to when this was largest for each feature. The absolute concentration of plasma ALT at T6 (the peak of the response) is also included. The order of features was determined by hierarchical clustering and the associated dendrogram is shown at the top of the heatmap. (**B**) Correlation between ALT concentration and the activation of innate-like and adaptive T cells at T6. Loess regression line is shown in black and the 95% confidence intervals in grey.

295 cohort were then combined at each time-point for GO term enrichment. Crucially, information
296 was retained to indicate what fraction of associated genes for each GO term derived from *P.*
297 *vivax* or *P. falciparum* infected volunteers. At diagnosis we found 289 GO terms of which 282
298 (97.58%) were shared almost equally between cohorts (figure 7A). ClueGO network
299 construction then revealed that these shared GO terms organised into functional groups
300 related to myeloid cell activation and systemic inflammation (figure 7B). Remarkably, we
301 found only 7 GO terms (2.42%) with associated genes that majoritively (> 65%) derived from
302 one volunteer cohort. All of these cohort-specific GO terms were located in the same region
303 of the ClueGO network and were enriched in volunteers infected with *P. vivax* - this
304 response was characterised by downregulation of structural ribosomal gene expression,
305 which can be induced by type I interferon signalling (62). Despite this difference, these
306 results show that the functional consequences of the innate immune response are highly
307 conserved between two divergent parasite species, which differ in host cell tropism, red cell
308 remodelling, tissue sequestration and in their potential to cause severe disease.

309 To examine parasite species-specific differences in the adaptive immune response to
310 malaria we repeated this analysis at T6. In contrast to diagnosis, only 151/235 (64.3%) GO
311 terms were shared between volunteer cohorts at this time-point (figure 7C). These shared
312 features related to nuclear activities involved in cell division, such as sister chromatid
313 segregation and mitotic spindle organization (figure 7D). On the other hand, 84/235 (35.7%)
314 GO terms were predominantly derived from just one dataset (*P. falciparum*) and these terms
315 were accessory to cell division, such as DNA replication and mitotic cell cycle phase
316 transition. It is therefore apparent that in both datasets the predominant transcriptional
317 signature six days post-treatment is one of cell division but the transcriptional changes
318 induced by *P. falciparum* are significantly more pronounced. This may indicate that *P.*
319 *falciparum* can induce lymphocyte activation on a scale in excess even of *P. vivax*.

320 To explore this possibility we examined the induction of signature genes associated with T
321 cell activation and differentiation in whole blood (figure 8A). Remarkably, we could detect the
322 upregulation of all major hallmarks of T_H1 polarisation (including T-bet and IFNγ) in
323 volunteers infected with *P. falciparum* (but not *P. vivax*). We then directly compared the
324 activation of $CD4^+$ T cells between volunteers by CyTOF (figure 8B-C). Whole blood
325 samples were collected, preserved and processed for mass cytometry in exactly the same
326 way during the VAC069A and VAC063C trials. FlowSOM clustering was performed
327 independently for each cohort and we summed all activated ($CD38^{hi}Bcl2^{lo}$) clusters to
328 measure the relative size of the adaptive response. This analysis clearly showed that *P.*
329 *falciparum* drives increased activation of $CD4^+$ and regulatory T cells in malaria-naive hosts.

330 In summary, the acute phase response that leads to systemic inflammation and coagulation
331 is shared between falciparum and vivax malaria, despite vast differences in parasite biology,
332 pathology and epidemiology. This suggests that innate cells do not differentiate between
333 parasite species and simply launch a hardwired programme of activation. In agreement,
334 every plasma analyte significantly upregulated in naive hosts infected with *P. vivax* (figure
335 1D) is also upregulated during CHMI with *P. falciparum* (VAC063C, Muñoz Sandoval *et al.*,
336 in preparation). In contrast, the adaptive immune response (measured after drug treatment
337 and the release of lymphocytes from inflamed tissues) differs markedly. Our data indicate

338 that *P. falciparum* drives increased $CD4^+$ T cell activation as compared to *P. vivax*, which is
339 already capable of activating one quarter of the entire T cell compartment.

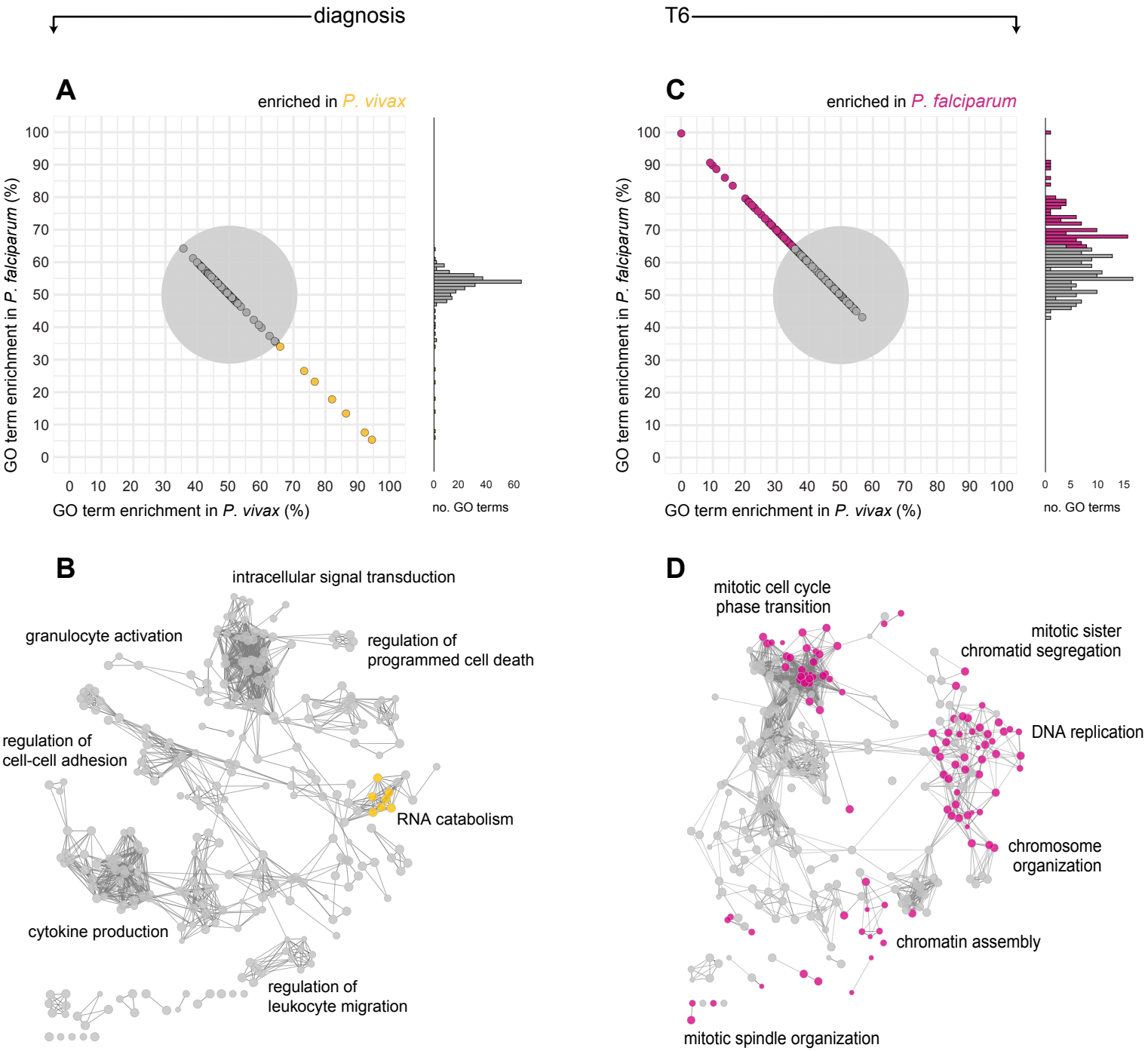

Figure 7 | The innate response to malaria does not distinguish parasite species. Whole blood RNA-sequencing was performed analogously during the VAC069A (*P. vivax*) and VAC063C (*P. falciparum*) CHMI studies (n = 6 and 3, respectively). Differentially expressed genes in *P. vivax* and *P. falciparum* were combined for GO analysis at diagnosis (A and B) or T6 (C and D). (**A** and **C**) Each GO term is represented by a point whose position on the x and y axis is determined by what proportion of associated genes were differentially expressed in volunteers infected with *P. vivax* or *P. falciparum*, respectively. The grey circle represents a 65% threshold that needed to be crossed to call a GO term as majoritively associated with one volunteer cohort. Because many points overlap around 50% a histogram of the number of GO terms is also shown along the y axis. All points and bars are coloured according to enrichment. (**B** and **D**) ClueGO networks of the GO terms represented in (A and C); nodes are coloured according to enrichment in *P. vivax* or *P. falciparum*. For each of the major functional groups a representative GO term was chosen as group name.

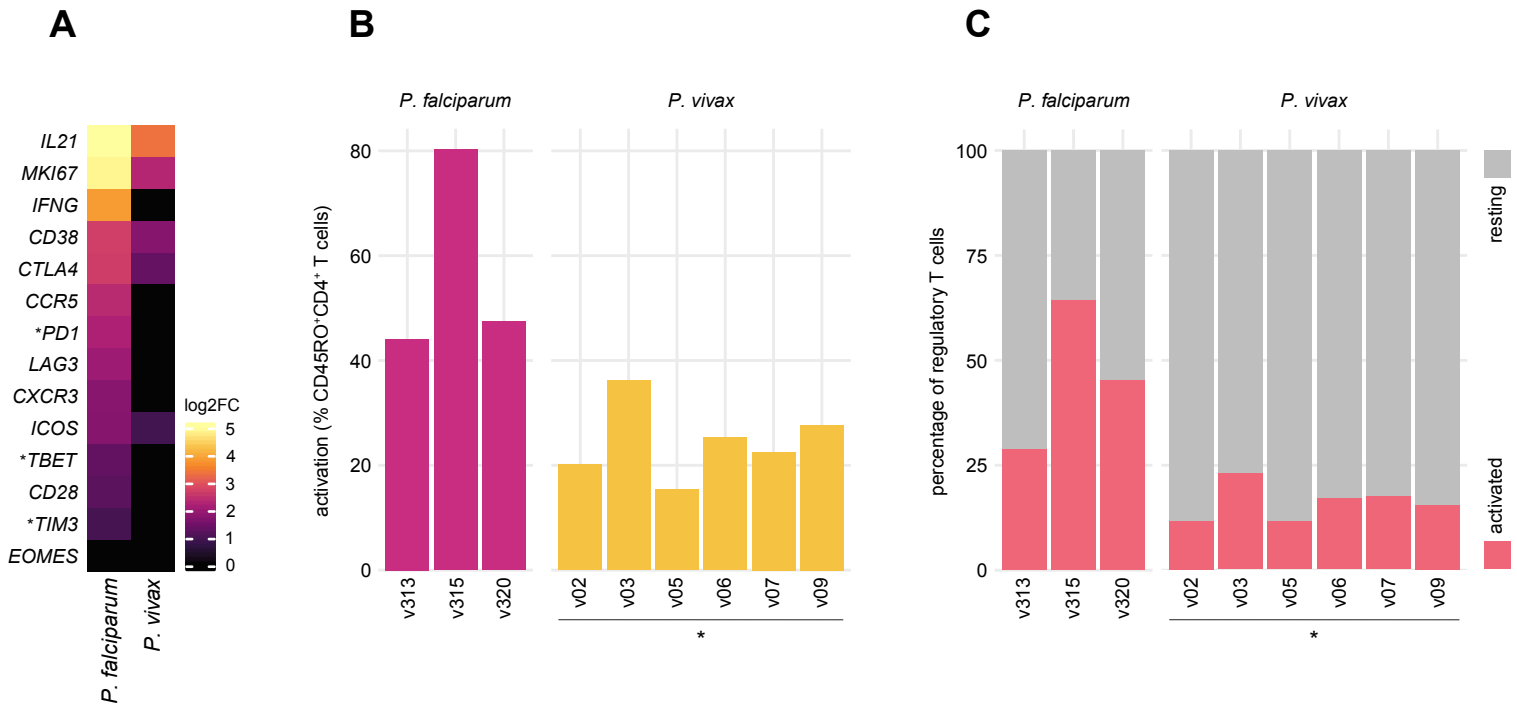

Figure 8 | Parasite species regulates CD4⁺ T cell activation. (**A**) Heatmap of signature T cell genes showing their log2 fold change at T6 (relative to baseline) in whole blood; asterisks indicate that common gene names were used. Genes that were not differentially expressed (adj p > 0.05) are shown with a fold change of zero. (**B**) Proportion of non-naive (CD45RO⁺) CD4⁺ T cells that are activated ($CD38^{hi}Bcl2^{lo}$) at T6 in volunteers infected with either *P. falciparum* or *P. vivax* by CHMI. (**C**) Proportion of regulatory T cells that are activated at T6 in volunteers infected with *P. falciparum* or *P. vivax*. In (B and C) FlowSOM was used to identify activated T cell clusters ($CD38^{hi}Bcl2^{lo}$) independently in each volunteer cohort; the frequency of activated clusters were summed and are shown as a proportion of the indicated lineage (analogous to figure 5C). Note that all volunteers were malaria-naive and therefore experienced a first-in-life infection. * p = 0.02381 Wilcoxon rank sum exact test (two-tailed).

340 ## Discussion

341 The innate immune response to *P. vivax* and *P. falciparum* appears to be indistinguishable
342 at a functional RNA and protein level. Both responses are dominated by activation of
343 myeloid cells, likely driven by interferon signalling, the abundant release of diverse
344 proinflammatory molecules, leukocyte migration, coagulation and hallmark signs and
345 symptoms of clinical malaria. Circulating monocytes and neutrophils are largely recent
346 emigrants from the bone marrow and recent studies have shown that innate priming during
347 the blood-stage of infection first occurs in this tissue (44, 63). *P. vivax* and *P. falciparum*
348 differ significantly in their genome composition, host cell tropism and prevalence in the bone
349 marrow (64, 65); that these differences have no apparent bearing on the initiation of
350 systemic inflammation is surprising and suggests that the emergency myeloid response is
351 hardwired. This finding is analogous to our recent report that two genetically distinct *P.*
352 *chabaudi* clones, which vary markedly in their capacity to sequester and cause
353 hyperparasitaemia and severe disease, trigger near-identical myeloid responses in the bone
354 marrow and spleen (66).

355 These data have important implications for studies that attempt to resolve drivers of severe
356 malaria. First, if there is no difference between *P. vivax* and *P. falciparum* in how they
357 activate the innate immune system then innate responses are unlikely to be sufficient for the
358 severe manifestations of disease, an outcome largely confined to falciparum malaria. That is
359 not to say that innate inflammation does not promote severe disease but instead point out
360 that excessive innate responses must be driven by additional extrinsic factors, such as
361 pathogen load (generally higher with *P. falciparum* (67, 68)) or T cell activation. Second,
362 studying activation of innate immune cells in the circulation (and the abundance of systemic
363 inflammatory markers) is not a good indicator of tissue-specific responses. This is evidenced
364 by the clear disconnect we identify between systemic inflammation and the level of T cell
365 activation and tissue damage measured after resolution of the acute phase response. This
366 finding could in part explain why the association between inflammatory markers measured in
367 blood and disease outcome are often so contradictory in endemic settings (69). We therefore
368 suggest that field studies should examine the function and fate of adaptive immune cells
369 when they return to the circulation and this can be readily achieved by extending sampling
370 for immune profiling beyond drug treatment.

371 We found innate-like and adaptive T cells express a broad range of activation markers and
372 the marker combination $CD38^{hi}Bcl2^{lo}$ was sufficient to identify activated cells in every
373 lineage. Cumulatively, the activated fraction of total T cells far exceeds what has been
374 reported for other human pathogens (50, 51); this indicates that T cells are indiscriminately
375 activated by malaria parasites. In this context, it is particularly significant that MAIT cells
376 were activated since they do not recognise peptide antigens loaded onto MHC molecules;
377 instead, they recognise riboflavin metabolite-derived antigens presented by APCs
378 expressing MR1 (70). *Plasmodium spp.* lack the pathways for riboflavin synthesis,
379 suggesting that MAIT cells are not responding in an antigen-specific manner. These innate-
380 like cells can act as sensors of tissue inflammation and be directly activated by cytokines
381 such as IL-12 and IL-18 (61, 71, 72). Adaptive T cells can also be activated and clonally

382 expand via this route (59, 60, 73). Our data therefore raise the intriguing possibility that *P.*
383 *vivax* triggers polyclonal bystander T cell activation in naive hosts. TCR sequencing has
384 shown polyclonal expansion of effector $CD4^+$ T cells in *Plasmodium chabaudi*, which lends
385 support to this hypothesis (74).

386 $CD4^+$ T cells dominated the adaptive response to *P. vivax* and all significant clusters had a
387 memory phenotype 6-days after drug treatment. But are these *bona fide* memory cells? This
388 may depend upon their antigen specificity; if all activated $CD4^+$ T cells recognise
389 *Plasmodium* epitopes then they may simply be short-lived effectors and the number that
390 persist to form a memory reservoir would need to be quantified further into convalescence.
391 On the other hand, if $CD4^+$ T cells specific for other pathogens (or vaccine epitopes) are
392 activated this might indicate clonal expansion of pre-existing memory cells (58). Compared
393 to naive T cells, memory cells are more easily activated in the absence of TCR signals (75) -
394 future studies should therefore prioritise investigating the antigen specificity and clonality of
395 activated T cells in human malaria. In the meantime, our data show that (regardless of
396 specificity) the differentiation of $CD4^+$ T cells towards an inflammatory T_H1 fate is a common
397 outcome of infection in naive hosts; this is evident in the widespread expression of T-bet,
398 Ki67, ICOS and CD28 in activated cells. Although most activated cells also expressed the
399 inhibitory receptors PD1 and CTLA4 this is now recognised to be an essential mechanism of
400 self-regulation (52, 53) - expression of PD1 cannot therefore serve as shorthand for T cell
401 exhaustion in malaria. Surprisingly, the major activated $CD4^+$ T cell cluster displayed a
402 $CD27^-$ cytotoxic phenotype; cells pushed down this route of differentiation typically arise in
403 the context of chronic stimulation or in autoinflammatory diseases (54-57). These data
404 therefore highlight the potency of the tissue environment for driving T cell activation in vivax
405 malaria.

406 More broadly, our data highlight the heterogeneity of activated $CD4^+$ T cells; clustering
407 identified at least five distinct populations, which underlines the power of high-dimensional
408 cytometry in uncovering cell fates that can easily be missed when relying on just a few
409 markers to define complex phenotypes. Future studies that incorporate additional
410 transcription factors and intracellular cytokines in the staining panel are likely to reveal even
411 richer functional diversity. Furthermore, the results presented in this study reveal only the
412 conserved T cell responses that are shared between volunteers. Human T cells are
413 inherently plastic (76) and there is enormous variation in the immune response to pathogens
414 and their products (77, 78). Immune variation is therefore likely to play a key role in
415 determining disease outcome in human malaria (35) and future studies can address this
416 point by increasing sample size and applying individual (rather than group-level) analysis
417 techniques to study T cell fates.

418 This study had a number of additional limitations. We cannot exclude effects of drug
419 treatment as a confounding variable at post-treatment time-points. Direct xenobiotic effects
420 seem unlikely to drive the T cell activation we observe, however, as artemisinin and its
421 derivatives have been shown to inhibit T cell responses in a dose-dependent manner both *in*
422 *vitro* and *in vivo* (79, 80). Drug treatment is also unlikely to explain the increase in ALT
423 observed in most volunteers. Liver injury is a common feature of clinical and experimental
424 malaria and occurs independently of the drug used or the treatment regime (32-34).
425 Furthermore, abnormal ALT levels significantly decrease 7-days after drug treatment in

426 patients with severe malaria (81), suggesting that infection or inflammation is the driver of
427 hepatocellular death. Of note, there were no significant deviations in albumin or bilirubin in
428 our volunteer cohort (Minassian *et al.*) indicating that the biosynthetic and metabolic
429 functions of the liver have not been compromised. Elevations in ALT are therefore a marker
430 of asymptomatic collateral tissue damage in CHMI, as previously suggested (33). Another
431 limitation of this study is that infections had to be terminated at a parasite density much
432 lower than would be observed in endemic settings. It is possible (perhaps likely) that we
433 would have found the innate immune response to *P. vivax* and *P. falciparum* diverge later in
434 infection although this would not contradict our conclusion that innate cells have no intrinsic
435 capacity to differentiate between parasite species. It is also unclear whether the levels of T
436 cell activation observed here can be maintained in infections of longer duration, or how
437 chronic infection would alter T cell function.

438 Our data nevertheless indicate that early in infection *P. falciparum* exceeds the already
439 prolific *P. vivax* in triggering $CD4^+$ T cell activation and proliferation independently of
440 pathogen load. This is evidenced by the remarkable transcriptional signature of T_H1
441 polarisation in whole blood when volunteers are infected with *P. falciparum* (but not *P. vivax*)
442 despite using the same study end-points. Moreover, $CD4^+$ T cell activation (including
443 regulatory T cells) was closely associated with tissue damage (ALT). As such, if *P.*
444 *falciparum* is better able to drive T cell activation and tissue damage in naive hosts then it is
445 tempting to speculate that this may be one way in which falciparum malaria causes more
446 severe disease (82).

447 Finally, all volunteers recruited to this study were malaria-naive and so some of the features
448 we describe here could be specific to first-in-life infections. This is conceivable since both
449 epidemiological and experimental data indicate that first infection differs from reinfection in
450 regards to the pyrogenic threshold (22, 83) and likelihood of severe malaria (84). In this
451 context, human rechallenge models may reveal how the immune response evolves to
452 repeated infections and could identify adaptations that coincide with clinical immunity. This
453 would be a powerful and complementary approach to the comparison of human T cell
454 responses between *P. vivax* and *P. falciparum*. And together these approaches to
455 experimental medicine may help resolve the immune mechanisms that can reduce disease
456 burden.

457 # Methods

458 **Clinical Trial Design**

459 Six volunteers were recruited to test the infectivity and safety of a new cryopreserved
460 stabilate containing a clonal field isolate of *P. vivax* (PvW1); this stabilate had carefully been
461 prepared for use in CHMI by blood challenge (Minassian *et al.*). These six volunteers were
462 enrolled into the VAC069 study and termed cohort A; the CHMI trial itself was named
463 VAC069A. VAC069A was sponsored by the University of Oxford, received ethical approval
464 from UK NHS Research Ethics Service (South Central - Hampshire A reference 18/SC/0577)
465 and was registered on ClinicalTrials.gov (NCT03797989). The trial was conducted in line
466 with the current version of the Declaration of Helsinki 2008 and conformed with the ICH
467 Guidelines for Good Clinical Practice.

468 The VAC069A trial is reported in full in the accompanying article by Minassian *et al.* In brief,
469 cryopreserved vials of stabilate were thawed, washed and diluted under aseptic conditions,
470 and then administered to healthy malaria-naive adult volunteers by intravenous injection.
471 Volunteers each received an inoculum containing between 116 and 2232 PvW1 genome
472 copies; variation in copy number had no measurable effect on parasite multiplication rate
473 (supplementary file 1). It is important to note that parasite dose may influence the time to
474 diagnosis but has no effect on outcome of infection in human malaria (85). After inoculation
475 whole blood was drawn twice daily to determine parasitaemia by qPCR (target gene = 18S
476 ribosomal RNA). Thick blood smears were also evaluated by experienced microscopists at
477 each time-point. Treatment was initiated once two diagnostic conditions were fulfilled:
478 parasitaemia above 5,000 parasite genome copies ml^{-1}, parasitaemia above 10,000 genome
479 copies ml^{-1}, positive thick blood smear and/or symptoms consistent with malaria. Treatment
480 usually consisted of artemether and lumefantrine (Riamet) or atovaquone and proguanil
481 (Malarone) if Riamet was contraindicated. Volunteer 05 received Malarone, all other
482 volunteers received Riamet.

483 All reported clinical symptoms (arthralgia, back pain, chills, diarrhoea, fatigue, fever,
484 headache, malaise, myalgia, nausea, pyrexia, rigor, sweating, vomiting) were recorded as
485 adverse events and assigned a severity score: 1 - transient or mild discomfort (no medical
486 intervention required); 2 - mild to moderate limitation in activity (no or minimal medical
487 intervention required); 3 - marked or severe limitation in activity requiring assistance (may
488 require medical intervention). At baseline, C7, C14 (if undiagnosed), diagnosis, T1 and T6
489 full blood counts and blood chemistry were evaluated at the Churchill and John Radcliffe
490 Hospital in Oxford, providing 5-part differential white cell counts and quantification of
491 electrolytes, urea, creatinine, bilirubin, alanine aminotransferase (ALT), alkaline phosphatase
492 (ALP) and albumin.

493 Blood for immunological analyses was collected in EDTA tubes by venepuncture at the
494 indicated time-points. All samples were processed immediately for downstream applications
495 in a laboratory adjacent to the clinical facility.

496 **Multiplexed plasma analyte analysis**

497 Whole blood was centrifuged at 1000g for 5 minutes to separate cellular components and
498 plasma. Plasma was then aspirated and centrifuged at 2000g for 10 minutes to remove
499 platelets. Avoiding the pellet, supernatants were aliquoted and snap-frozen on dry ice before
500 storage at -80°C until further processing. Plasma samples from baseline, diagnosis, T6 and
501 45-days post-challenge (memory phase) were thawed on ice before centrifuging at 1000g for
502 1 minute to remove potential protein aggregates. The concentration of 39 different analytes
503 was then measured by running every sample across four different custom Legendplex
504 assays from Biolegend, according to the manufacturer's instructions. Filter plates with
505 samples and concentration standards were then acquired on a LSRFortessa flow cytometer
506 (BD). FCS files were processed using Legendplex software (version 7.1), which
507 automatically interpolates a standard curve using the plate-specific standards and calculates
508 analyte concentrations for each sample. Samples from v09 were excluded after failing QC
509 and statistical analysis of the remaining 5 volunteers was carried out in R (version 3.6.3).
510 Using *stats*, linear models were fit using restricted maximum likelihood for each analyte with
511 log10 transformed analyte concentrations as response variable and time-point and volunteer
512 as categorical fixed effects. Linear hypothesis testing via pairwise comparisons was
513 performed using *multcomp*'s glht function and adjusted for multiple testing (Benjamini &
514 Hochberg). An FDR < 0.05 was considered significant. Results were visualised using
515 *ComplexHeatmap* (86), inspired by the plotDiffHeatmap function of *CATALYST* (87) and
516 *ggplot2* (88).

517 **RNA-sequencing and data analysis**

518 Whole blood was added to Tempus reagent (Applied Biosystems) at a ratio of 1:2 within 60-
519 minutes of blood draw before storage at -80°C. RNA extraction was performed using the
520 Tempus Spin RNA isolation reagent kit (Applied Biosystems) according to the
521 manufacturer's instructions. Briefly, lysed blood samples were thawed and centrifuged at
522 3000g for 30 minutes at 4°C to pellet nucleic acids. Pellets were resuspended in RNA
523 purification re-suspension solution and centrifuged on a silica column to remove non-nucleic
524 acid contaminants. After washing, the column was incubated for two minutes at 70°C before
525 eluting nucleic acids. The eluate was then subjected to DNA digestion using the RNA Clean
526 and Concentrator-5 kit (Zymo Research). Purified RNA was eluted in 30*µ*l DNAse/RNAse-
527 free water; quantification and quality control were carried out on a Qubit (Thermo Fisher
528 Scientific) and Bioanalyzer (Agilent Technologies), respectively. All samples were diluted to
529 a concentration of approximately 20-40 ng/*µ*l and shipped to the Wellcome Sanger Institute
530 for library preparation and sequencing. Libraries were constructed using the NEBNext® Ultra
531 II™ RNA library prep kit on an Agilent Bravo WS automation system followed by 14 cycles of
532 PCR using KAPA HiFi HotStart DNA polymerase. Libraries were then pooled in equimolar
533 amounts and 75bp paired end (PE) reads were generated on the Illumina HiSeq v4
534 according to the manufacturer's standard protocol (~ 35 million PE reads per sample).

535 FASTQ files were quality assessed using FASTQC, reads were aligned to the human
536 transcriptome (Ensembl, release 98) using bowtie2 (v2.2.7) (89) and after alignment globin
537 reads were discarded. DESeq2 (39) was used for all differential gene expression analysis;

538 differentially expressed genes were classified as those with an adj $p < 0.05$ and an absolute
539 fold change > 1.5. To visualise differentially expressed genes in the heatmap in figure 8A all
540 genes with multiple differentially expressed transcripts were filtered to retain the transcript
541 with the lowest adj p value - this was taken forward to estimate fold change.

542 Gene ontology analysis was performed on lists of differentially expressed genes in
543 Cytoscape (version 3.8.0 using Java 11.0.9.1 in Ubuntu) using the ClueGO plugin (version
544 2.5.7) (40, 41). The ontologies GO Biological Process-EBI-uniprot-GOA (updated
545 08.05.2020) and GO Molecular Function-EBI-uniprot-GOA (updated 08.05.2020) were both
546 used. ClueGO networks were constructed using GO term levels 5-11, GO fusion = true and
547 a lower cut-off of 3 genes (or 5% associated genes). The lower bound for connecting GO
548 terms with shared genes was set at a kappa score of 0.4.

549 **CyTOF sample acquisition**

550 Whole blood samples were taken at baseline, C10, diagnosis and T6 and stabilised in whole
551 blood preservation buffer (Cytodelics AB) within 30 minutes of blood draw. Preserved
552 samples were stored at -80°C. Samples were thawed in a water bath at 37°C and then fixed
553 and red cells lysed using the whole blood preservation kit (Cytodelics AB) according to the
554 manufacturer's instructions. Fixed samples were washed, permeabilised and barcoded using
555 the Cell-ID 20-Plex Pd Barcoding Kit (Fluidigm). Barcoded samples were then pooled and
556 counted before resuspending in cell staining buffer (Fluidigm) at 40 x 10^6 cells ml^{-1}. An equal
557 volume of freshly prepared surface antibody cocktail (supplementary file 2) was added for 30
558 minutes and incubated at room temperature under gentle agitation. After washing, samples
559 were resuspended in nuclear antigen staining buffer for 30 minutes at room temperature
560 under gentle agitation. Samples were then washed in nuclear antigen staining perm buffer
561 (Fluidigm) before antibodies for nuclear targets were added and incubated for a further 45
562 minutes. After another round of washing cells were fixed using 1.6% paraformaldehyde in
563 PBS for 10 minutes and then finally resuspended in fix and perm buffer (Fluidigm) and 72.5
564 nM Cell-ID™ 191Ir/193Ir intercalator (Fluidigm) at a concentration of 2 x10^6 cells ml^{-1}. Cells
565 were incubated overnight at 4°C.

566 Sample acquisition was performed on a freshly tuned Helios mass cytometer (Fluidigm)
567 using the WB injector and acquired with 10% normalisation beads (140Ce, 151Eu, 165Ho,
568 and 175Lu, all Fluidigm). Both staining and sample acquisition were carried out in two
569 batches (all time-points for 3 volunteers per batch). On each acquisition day, pooled cells
570 were counted again before removing an aliquot of 2 x 10^6 cells; aliquots were washed twice
571 in cell staining buffer and resuspended in 1ml cell acquisition solution (Fluidigm). Each
572 aliquot was acquired completely before washing and processing the next aliquot until all
573 pooled samples had been acquired. Cells were acquired at a rate of 300-500 events per
574 second.

575 **CyTOF data analysis**

576 FCS files were generated using CyTOF software (version 6.7, Fluidigm) followed by
577 normalisation (90) and debarcoding (91) using the *CATALYST* workflow described in (92).
578 Single-stained beads were used for compensation (using non-negative linear least squares
579 regression (93)) and FCS files were gated in the Cytobank web portal (Beckmann Coulter) to
580 exclude normalisation beads and doublets. Singlet T cells ($CD45^{+}CD3^{+}CD19^{-}$) were taken
581 forward for analysis. Intensity distributions of each channel were inspected to remove
582 channels of low variance (CD14, Tim3, Integrin β7, CD56, CD16, CD49d, CD103, CXCR5).
583 Of note, low variance in these channels does not necessarily reflect uniform or absent
584 expression of these markers, but could also be due to inefficient staining of fixed samples
585 using these antibody clones. The remaining 28 markers were used for both UMAP
586 projections and FlowSOM clustering.

587 UMAP (46) creates low-dimensional projections of high-dimensional data. Here cells were
588 grouped according to marker expression intensity and embedded in a 2D plane such that
589 phenotypic similarity within and between populations is preserved in the Euclidean distance
590 of the projection. We used its R implementation in the *scater* package (94), which in turn
591 relies on *uwot* (github.com/jlmelville/uwot). Features were scaled to unit variance and the 15
592 nearest neighbours were considered for embedding. UMAP coordinates were then exported
593 for visualisation using *ggplot2*.

594 FlowSOM (47) uses self-organising maps (SOM) to efficiently categorise cytometry data into
595 non-overlapping cell populations. Clustering was performed with a target cluster number of
596 100 and metaclustering with a target cluster number of 45. This approach purposefully
597 overclustered the data to resolve potentially small subsets, a trade-off that can split
598 phenotypically similar cells into more than one population (95). Overclustering was
599 addressed by manual inspection of all clusters and merging of phenotypically similar
600 populations. After manual merging, each T cell was classified into one of 34 unique clusters.
601 Names were assigned manually using activation, lineage and memory markers to broadly
602 categorise each T cell cluster (see supplementary figure 2); when more than one cluster was
603 placed into the same category clusters were given an accessory label to highlight their
604 unique phenotype or property (e.g. skin-homing, indicated by the expression of CLA). The
605 R/Bioconductor package *ComplexHeatmap* was used to visualise T cell cluster phenotypes;
606 the arcsine transformed signal intensity of each marker was independently scaled using a 0-
607 1 transformation across all 34 clusters.

608 For differential abundance analysis we followed the workflow laid out in (92). FlowSOM
609 cluster cell counts were modelled linearly with time-point as a dependent categorical variable
610 and volunteer as a fixed effect using the *diffcyt* (49) implementation of edgeR (48). The
611 edgeR functions automatically normalise cluster counts for the total number of cells and
612 improve statistical power by sharing information on cluster count variance between clusters.
613 Pairwise comparisons were performed relative to baseline, and clusters with an FDR < 0.05
614 and absolute fold change > 2 were deemed to vary significantly through time.

615 **Pearson correlation analysis**

616 The fold change of each T cell cluster and plasma analyte was calculated using raw cluster
617 percentages or plasma concentrations, respectively. For each feature, these were calculated
618 at diagnosis or T6 (relative to baseline) according to their largest absolute fold change. All
619 data were log2 transformed and Pearson correlation was performed using the cor function
620 from the *stats* R package. Correlation coefficients were then used for hierarchical clustering
621 by Euclidean distance using *ComplexHeatmap*.

622 **Comparing the immune response between *P. vivax* and *P. falciparum***

623 For the comparison of *P. vivax* and *P. falciparum* data from a previously conducted clinical
624 trial (VAC063C) were used; the VAC063C trial is reported in full elsewhere (Muñoz Sandoval
625 *et al.*, in preparation). In brief, three healthy malaria-naive adult volunteers were inoculated
626 with *P. falciparum* (clone 3D7) by routine blood challenge (approx. 800 parasites per
627 volunteer) (96). Starting one day after infection volunteers attended clinic for assessment
628 and blood sampling every 12-hours, and parasite density was measured in real time by
629 qPCR (target gene = 18S ribosomal RNA). At diagnosis (asymptomatic with parasitaemia
630 above 10,000 parasites ml^{-1} or symptomatic with parasitaemia above 5000 parasites ml^{-1})
631 volunteers were treated with either Riamet or Malarone. VAC063C was sponsored by the
632 University of Oxford, received ethical approval from UK NHS Research Ethics Service
633 (South Central - Oxford A reference 18/SC/0521) and was registered on ClinicalTrials.gov
634 (NCT03906474).

635 Blood for immunological analyses was collected in EDTA tubes by venepuncture at baseline,
636 during infection, diagnosis, T6 and 45-days post-challenge (memory phase). To undertake
637 whole blood RNA-sequencing samples were processed exactly as described above for *P.*
638 *vivax* CHMI. Libraries were then prepared using the TruSeq Stranded mRNA library prep kit
639 (Illumina) and sequenced on the NovaSeq 6,000 Illumina platform to yield 50 bp paired end
640 (PE) reads. Data processing and analysis was carried out analogously to VAC069A to
641 identify differentially expressed genes at diagnosis and T6 (versus baseline). ClueGO
642 networks were constructed by combining separate lists of differentially expressed genes
643 from volunteers infected with *P. vivax* and *P. falciparum*. For each GO term information on
644 what fraction of associated genes were derived from the list of DEG in vivax or falciparum
645 malaria was retained. Any GO term containing > 65% associated genes from a single
646 volunteer cohort was considered to be enriched in that infection model, otherwise GO terms
647 were considered to be shared.

648 For CyTOF analysis whole blood samples were preserved, processed and acquired on a
649 Helios mass cytometer exactly as described for *P. vivax* CHMI. Data processing was also
650 performed analogously to VAC069A and FlowSOM was used to place each T cell into a
651 phenotypically unique cluster. Note that clustering was performed independently on the
652 VAC069A and VAC063C datasets. For each volunteer, the proportion of activated $CD4^{+}$ T
653 cells and regulatory T cells was then calculated by summing the frequency of all clusters
654 with a $CD38^{hi}Bcl2^{lo}$ phenotype.

Data access

RNA-sequencing data from VAC069A have been deposited in the European Genome-phenome Archive (EGA) and are accessible through accession number EGAS00001003847. RNA-seq data from VAC063C have been deposited in NCBI's Gene Expression Omnibus and are accessible through accession number GSE172450. CyTOF (mass cytometry) data are available at flowrepository.org and can be accessed through experiment number FR-FCM-Z3HA.

Acknowledgements

The authors would like to thank Mandy Sanders and the DNA Pipelines team at the Wellcome Sanger Institute for their support with RNA-seq library preparation and data production. We would also like to thank the VAC069A and VAC063C clinical and laboratory study teams for assistance (University of Oxford), and all of the clinical trial volunteers who participated in the studies.

Funding

The VAC069A trial was supported in part by funding from the European Union's Horizon 2020 research and innovation programme under grant agreement for MultiViVax (number 733073). The VAC063C trial was supported in part by the Office of Infectious Diseases, Bureau for Global Health, U.S. Agency for International Development (USAID) under the terms of the Malaria Vaccine Development Program (MVDP) Contract AID-OAA-C-15-00071, for which Leidos, Inc. is the prime contractor. The opinions expressed herein are those of the authors and do not necessarily reflect the views of the USAID. Both clinical studies were also supported in part by the National Institute for Health Research (NIHR) Oxford Biomedical Research Centre (BRC). The views expressed are those of the authors and not necessarily those of the NIHR or the Department of Health and Social Care. CyTOF data were generated in the mass cytometry facility at the Weatherall Institute of Molecular Medicine (University of Oxford), which is supported by MRC Human Immunology Unit core funding (MC_UU_00008) and the Oxford Single Cell Biology Consortium (OSCBC). FAB is the recipient of a Wellcome Trust PhD studentship (grant no. 203764/Z/16/Z). JCR and the DNA Pipelines team (Sanger) are supported by funding from the Wellcome Trust (grant no. 206194/Z/17/Z). SJD is a Jenner Investigator, the recipient of a Wellcome Trust Senior Fellowship (grant no. 106917/Z/15/Z) and a Lister Institute Research Prize Fellow. PJS is the recipient of a Sir Henry Dale Fellowship jointly funded by the Wellcome Trust and the Royal Society (grant no. 107668/Z/15/Z).

Declaration of interests

The authors declare no competing interests.

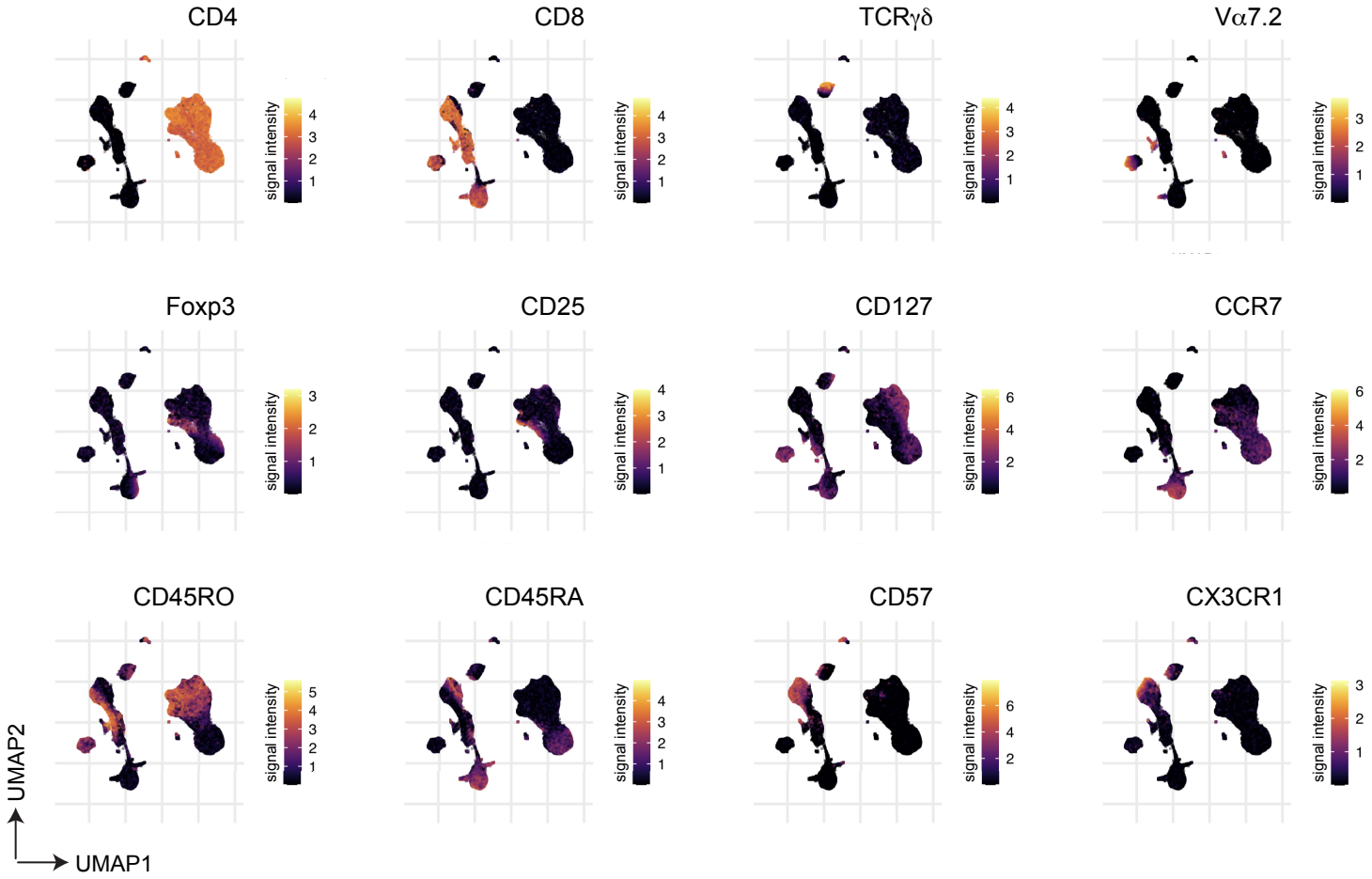

Supplementary figure 1 | Expression of lineage and memory markers across the UMAP projection. Data shown at T6; used to pinpoint the location of each major T cell subset. The arcsine transformed signal intensity is plotted for each marker.

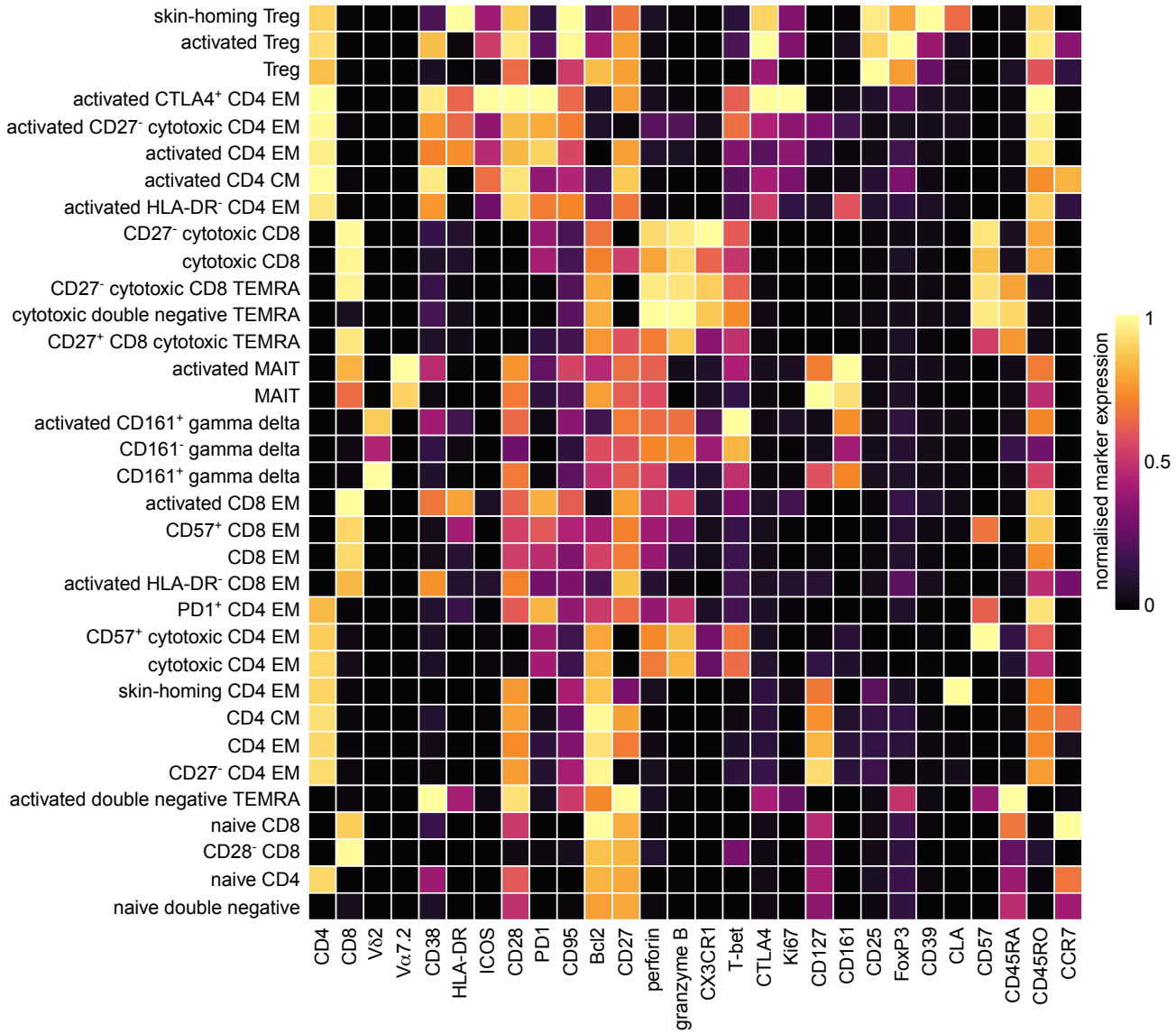

Supplementary figure 2 | Phenotype of each unique T cell cluster. Heatmap showing normalised median expression values of all markers used for clustering in each of the 34 T cell clusters. Names were assigned manually using activation, lineage and memory markers to broadly categorise each T cell cluster; when more than one cluster was placed into the same category (e.g. activated CD4 EM) clusters were given an accessory label to highlight their unique phenotype or property (e.g. skin-homing, indicated by the expression of CLA).

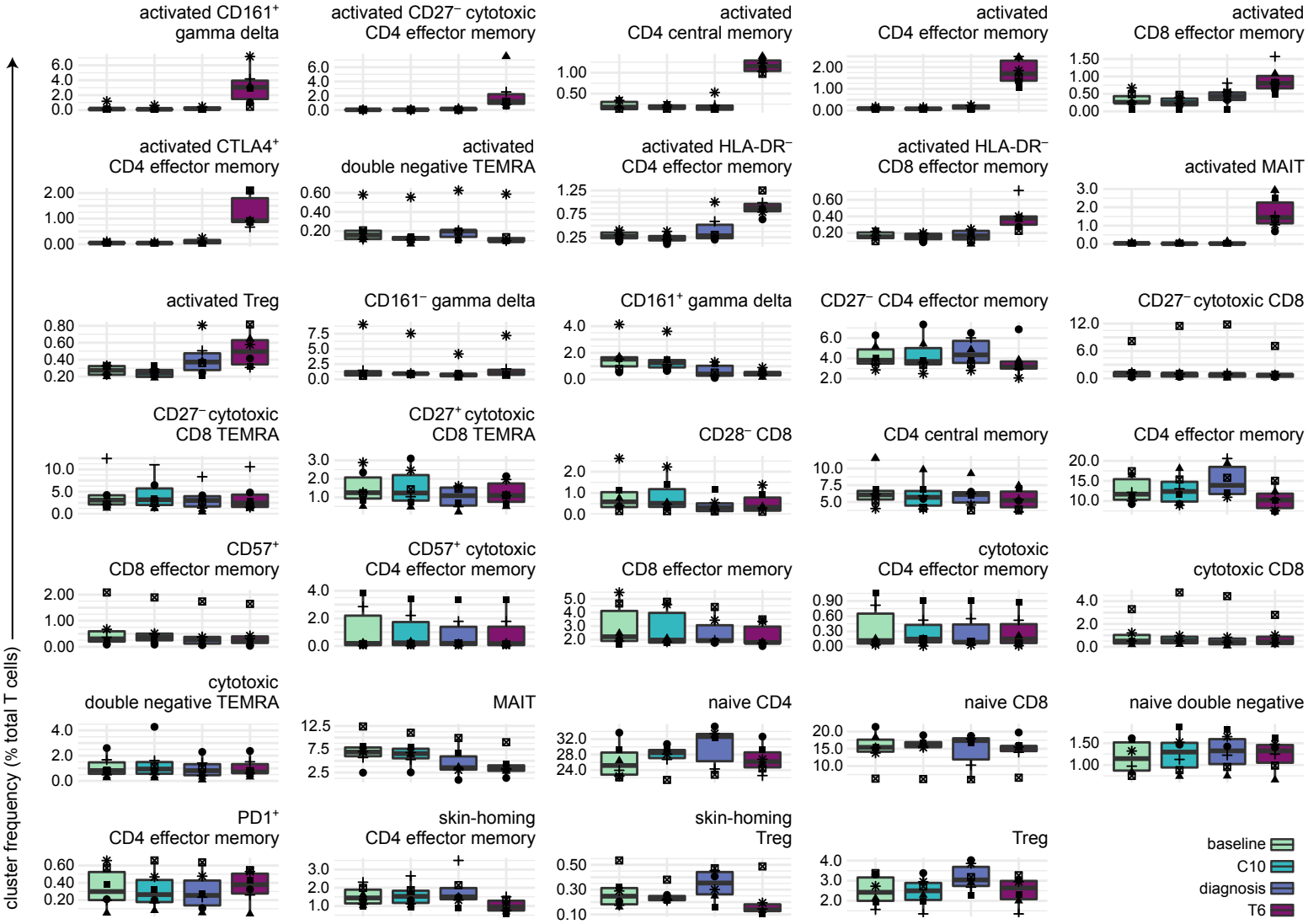

Supplementary figure 3 | Frequency of each T cell cluster during and after infection. Every unique T cell cluster is shown as the proportion of total T cells at each time-point.

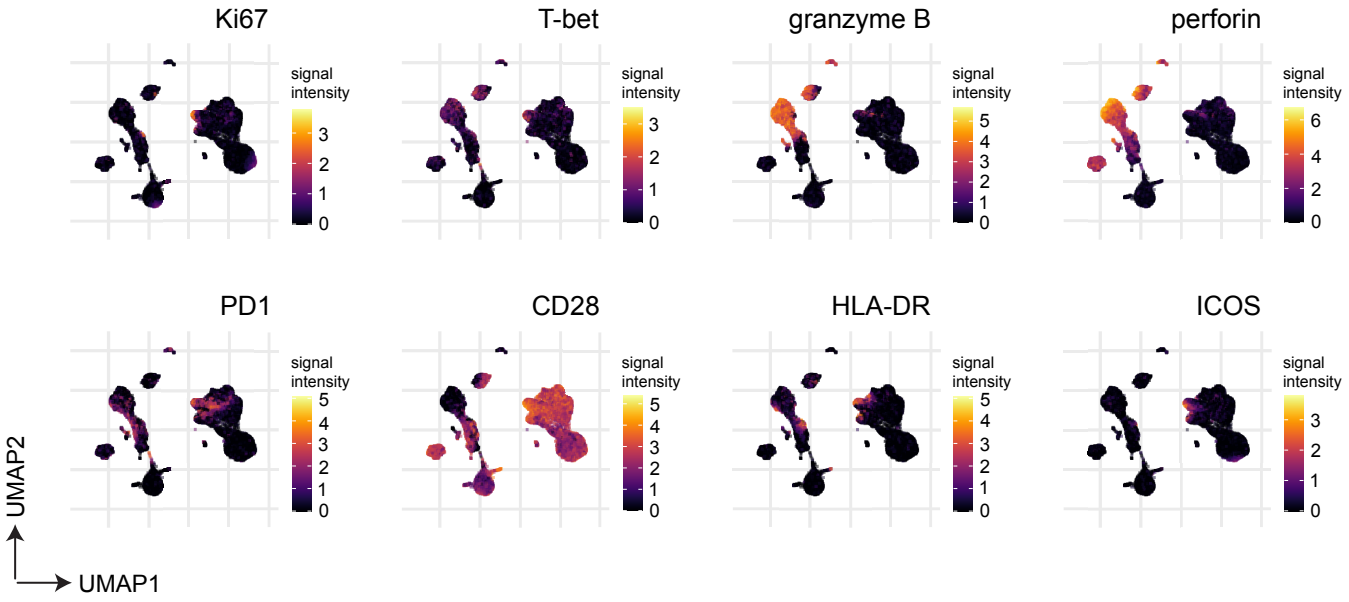

Supplementary figure 4 | Expression of activation, proliferation and differentiation markers across the UMAP projection. Data shown at T6; allows for a direct comparison of expression levels between activated $CD4^+$ T cells and all other T cell subsets. The arcsine transformed signal intensity is plotted for each marker.

690 Supplementary Files

691 **Supplementary file 1**. Demographics of volunteers infected with *Plasmodium vivax* (PvW1)
692 by blood challenge; includes genetic and non-genetic variables known to influence human
693 immune variation *in vitro*.

694 **Supplementary file 2**. Mass cytometry antibody panel for T cell fate and function in vivax
695 malaria; includes information on the antibody clone and heavy metal conjugate.

696 ## References

697 1. Battle KE, Lucas TCD, Nguyen M, Howes RE, Nandi AK, Twohig KA, Pfeffer DA,
698 Cameron E, Rao PC, Casey D, Gibson HS, Rozier JA, et al. Mapping the global endemicity
699 and clinical burden of Plasmodium vivax, 2000-17: a spatial and temporal modelling study.
700 Lancet. 2019;394(10195):332-43. PubMed PMID: 31229233.
701 2. Ley B, Luter N, Espino FE, Devine A, Kalnoky M, Lubell Y, Thriemer K, Baird JK,
702 Poirot E, Conan N, Kheong CC, Dysoley L, et al. The challenges of introducing routine
703 G6PD testing into radical cure: a workshop report. Malar J. 2015;14:377. PubMed PMID:
704 26416229.
705 3. Thriemer K, Ley B, Bobogare A, Dysoley L, Alam MS, Pasaribu AP, Sattabongkot J,
706 Jambert E, Domingo GJ, Commons R, Auburn S, Marfurt J, et al. Challenges for achieving
707 safe and effective radical cure of Plasmodium vivax: a round table discussion of the APMEN
708 Vivax Working Group. Malar J. 2017;16(1):141. PubMed PMID: 28381261.
709 4. Ashley EA, Recht J, White NJ. Primaquine: the risks and the benefits. Malar J.
710 2014;13:418. PubMed PMID: 25363455.
711 5. Thriemer K, Poespoprodjo JR, Kenangalem E, Douglas NM, Sugiarto P, Anstey NM,
712 Simpson JA, Price RN. The risk of adverse clinical outcomes following treatment of
713 Plasmodium vivax malaria with and without primaquine in Papua, Indonesia. PLoS Negl
714 Trop Dis. 2020;14(11):e0008838. PubMed PMID: 33175835.
715 6. Draper SJ, Sack BK, King CR, Nielsen CM, Rayner JC, Higgins MK, Long CA, Seder
716 RA. Malaria Vaccines: Recent Advances and New Horizons. Cell Host Microbe.
717 2018;24(1):43-56. PubMed PMID: 30001524.
718 7. Sharp PM, Plenderleith LJ, Hahn BH. Ape Origins of Human Malaria. Annu Rev
719 Microbiol. 2020;74:39-63. PubMed PMID: 32905751.
720 8. Sharma S, DeOliveira RB, Kalantari P, Parroche P, Goutagny N, Jiang Z, Chan J,
721 Bartholomeu DC, Lauw F, Hall JP, Barber GN, Gazzinelli RT, et al. Innate immune
722 recognition of an AT-rich stem-loop DNA motif in the Plasmodium falciparum genome.
723 Immunity. 2011;35(2):194-207. PubMed PMID: 21820332.
724 9. Parroche P, Lauw FN, Goutagny N, Latz E, Monks BG, Visintin A, Halmen KA,
725 Lamphier M, Olivier M, Bartholomeu DC, Gazzinelli RT, Golenbock DT. Malaria hemozoin is
726 immunologically inert but radically enhances innate responses by presenting malaria DNA to
727 Toll-like receptor 9. Proc Natl Acad Sci U S A. 2007;104(6):1919-24. PubMed PMID:
728 17261807.
729 10. Luxemburger C, Ricci F, Nosten F, Raimond D, Bathet S, White NJ. The
730 epidemiology of severe malaria in an area of low transmission in Thailand. Trans R Soc Trop
731 Med Hyg. 1997;91(3):256-62. PubMed PMID: 9231189.
732 11. Chan LJ, Dietrich MH, Nguitragool W, Tham WH. Plasmodium vivax Reticulocyte
733 Binding Proteins for invasion into reticulocytes. Cell Microbiol. 2020;22(1):e13110. PubMed
734 PMID: 31469946.
735 12. Gruszczyk J, Kanjee U, Chan LJ, Menant S, Malleret B, Lim NTY, Schmidt CQ, Mok
736 YF, Lin KM, Pearson RD, Rangel G, Smith BJ, et al. Transferrin receptor 1 is a reticulocyte-
737 specific receptor for Plasmodium vivax. Science. 2018;359(6371):48-55. PubMed PMID:
738 29302006.

739 13. Junqueira C, Barbosa CRR, Costa PAC, Teixeira-Carvalho A, Castro G, Sen Santara
740 S, Barbosa RP, Dotiwala F, Pereira DB, Antonelli LR, Lieberman J, Gazzinelli RT. Cytotoxic
741 CD8(+) T cells recognize and kill Plasmodium vivax-infected reticulocytes. Nat Med.
742 2018;24(9):1330-6. PubMed PMID: 30038217.
743 14. Handayani S, Chiu DT, Tjitra E, Kuo JS, Lampah D, Kenangalem E, Renia L,
744 Snounou G, Price RN, Anstey NM, Russell B. High deformability of Plasmodium vivax-
745 infected red blood cells under microfluidic conditions. J Infect Dis. 2009;199(3):445-50.
746 PubMed PMID: 19090777.
747 15. Obaldia N, 3rd, Meibalan E, Sa JM, Ma S, Clark MA, Mejia P, Moraes Barros RR,
748 Otero W, Ferreira MU, Mitchell JR, Milner DA, Huttenhower C, et al. Bone Marrow Is a Major
749 Parasite Reservoir in Plasmodium vivax Infection. mBio. 2018;9(3). PubMed PMID:
750 29739900.
751 16. Anstey NM, Handojo T, Pain MC, Kenangalem E, Tjitra E, Price RN, Maguire GP.
752 Lung injury in vivax malaria: pathophysiological evidence for pulmonary vascular
753 sequestration and posttreatment alveolar-capillary inflammation. J Infect Dis.
754 2007;195(4):589-96. PubMed PMID: 17230420.
755 17. Rahimi BA, Thakkinstian A, White NJ, Sirivichayakul C, Dondorp AM, Chokejindachai
756 W. Severe vivax malaria: a systematic review and meta-analysis of clinical studies since
757 1900. Malar J. 2014;13:481. PubMed PMID: 25486908.
758 18. Lin E, Kiniboro B, Gray L, Dobbie S, Robinson L, Laumaea A, Schopflin S, Stanisic
759 D, Betuela I, Blood-Zikursh M, Siba P, Felger I, et al. Differential patterns of infection and
760 disease with P. falciparum and P. vivax in young Papua New Guinean children. PLoS One.
761 2010;5(2):e9047. PubMed PMID: 20140220.
762 19. Michon P, Cole-Tobian JL, Dabod E, Schoepflin S, Igu J, Susapu M, Tarongka N,
763 Zimmerman PA, Reeder JC, Beeson JG, Schofield L, King CL, et al. The risk of malarial
764 infections and disease in Papua New Guinean children. Am J Trop Med Hyg.
765 2007;76(6):997-1008. PubMed PMID: 17556601.
766 20. Boyd MF. A review of studies on immunity to vivax malaria. J Natl Malar Soc.
767 1947;6(1):12-31. PubMed PMID: 20263110.
768 21. Ciuca M, Ballif L, Chelarescu-Vieru M. Immunity in malaria. Transactions of the Royal
769 Society of Tropical Medicine and Hygiene. 1934;27(6):619-22.
770 22. Collins WE, Jeffery GM, Roberts JM. A retrospective examination of reinfection of
771 humans with Plasmodium vivax. Am J Trop Med Hyg. 2004;70(6):642-4. PubMed PMID:
772 15211006.
773 23. Payne RO, Griffin PM, McCarthy JS, Draper SJ. Plasmodium vivax Controlled
774 Human Malaria Infection - Progress and Prospects. Trends Parasitol. 2017;33(2):141-50.
775 PubMed PMID: 27956060.
776 24. Bennett JW, Yadava A, Tosh D, Sattabongkot J, Komisar J, Ware LA, McCarthy WF,
777 Cowden JJ, Regules J, Spring MD, Paolino K, Hartzell JD, et al. Phase 1/2a Trial of
778 Plasmodium vivax Malaria Vaccine Candidate VMP001/AS01B in Malaria-Naive Adults:
779 Safety, Immunogenicity, and Efficacy. PLoS Negl Trop Dis. 2016;10(2):e0004423. PubMed
780 PMID: 26919472.
781 25. Collins KA, Wang CY, Adams M, Mitchell H, Robinson GJ, Rampton M, Elliott S,
782 Odedra A, Khoury D, Ballard E, Shelper TB, Lucantoni L, et al. A Plasmodium vivax
783 experimental human infection model for evaluating efficacy of interventions. J Clin Invest.
784 2020;130(6):2920-7. PubMed PMID: 32045385.

785 26. Herrera S, Fernandez O, Manzano MR, Murrain B, Vergara J, Blanco P, Palacios R,
786 Velez JD, Epstein JE, Chen-Mok M, Reed ZH, Arevalo-Herrera M. Successful sporozoite
787 challenge model in human volunteers with Plasmodium vivax strain derived from human
788 donors. Am J Trop Med Hyg. 2009;81(5):740-6. PubMed PMID: 19861603.
789 27. McCarthy JS, Griffin PM, Sekuloski S, Bright AT, Rockett R, Looke D, Elliott S,
790 Whiley D, Sloots T, Winzeler EA, Trenholme KR. Experimentally induced blood-stage
791 Plasmodium vivax infection in healthy volunteers. J Infect Dis. 2013;208(10):1688-94.
792 PubMed PMID: 23908484.
793 28. Hernandez-Castaneda MA, Happ K, Cattalani F, Wallimann A, Blanchard M, Fellay I,
794 Scolari B, Lannes N, Mbagwu S, Fellay B, Filgueira L, Mantel PY, et al. gammadelta T Cells
795 Kill Plasmodium falciparum in a Granzyme- and Granulysin-Dependent Mechanism during
796 the Late Blood Stage. J Immunol. 2020;204(7):1798-809. PubMed PMID: 32066596.
797 29. Riggle BA, Manglani M, Maric D, Johnson KR, Lee MH, Neto OLA, Taylor TE, Seydel
798 KB, Nath A, Miller LH, McGavern DB, Pierce SK. CD8+ T cells target cerebrovasculature in
799 children with cerebral malaria. J Clin Invest. 2020;130(3):1128-38. PubMed PMID:
800 31821175.
801 30. Spence PJ, Langhorne J. T cell control of malaria pathogenesis. Curr Opin Immunol.
802 2012;24(4):444-8. PubMed PMID: 22658628.
803 31. Stanisic DI, Cutts J, Eriksson E, Fowkes FJ, Rosanas-Urgell A, Siba P, Laman M,
804 Davis TM, Manning L, Mueller I, Schofield L. gammadelta T cells and CD14+ monocytes are
805 predominant cellular sources of cytokines and chemokines associated with severe malaria. J
806 Infect Dis. 2014;210(2):295-305. PubMed PMID: 24523513.
807 32. Chughlay MF, Akakpo S, Odedra A, Csermak-Renner K, Djeriou E, Winnips C,
808 Leboulleux D, Gaur AH, Shanks GD, McCarthy J, Chalon S. Liver Enzyme Elevations in
809 Plasmodium falciparum Volunteer Infection Studies: Findings and Recommendations. Am J
810 Trop Med Hyg. 2020;103(1):378-93. PubMed PMID: 32314694.
811 33. Odedra A, Webb L, Marquart L, Britton LJ, Chalon S, Moehrle JJ, Anstey NM,
812 William T, Grigg MJ, Lalloo DG, Barber BE, McCarthy JS. Liver Function Test Abnormalities
813 in Experimental and Clinical Plasmodium vivax Infection. Am J Trop Med Hyg.
814 2020;103(5):1910-7. PubMed PMID: 32815508.
815 34. Reuling IJ, de Jong GM, Yap XZ, Asghar M, Walk J, van de Schans LA, Koelewijn R,
816 Farnert A, de Mast Q, van der Ven AJ, Bousema T, van Hellemond JJ, et al. Liver Injury in
817 Uncomplicated Malaria is an Overlooked Phenomenon: An Observational Study.
818 EBioMedicine. 2018;36:131-9. PubMed PMID: 30243492.
819 35. Milne K, Ivens A, Reid AJ, Lotkowska ME, O'Toole A, Sankaranarayanan G, Munoz
820 Sandoval D, Nahrendorf W, Regnault C, Edwards NE, Silk SE, Payne RO, et al. Mapping
821 immune variation and var gene switching in naive hosts infected with Plasmodium
822 falciparum. medRxiv (doi:101101/2020090420188144). 2020.
823 36. Francischetti IM, Seydel KB, Monteiro RQ. Blood coagulation, inflammation, and
824 malaria. Microcirculation. 2008;15(2):81-107. PubMed PMID: 18260002.
825 37. Angchaisuksiri P. Coagulopathy in malaria. Thromb Res. 2014;133(1):5-9. PubMed
826 PMID: 24099998.
827 38. Meltzer E, Keller S, Shmuel S, Schwartz E. D-dimer levels in non-immune travelers
828 with malaria. Travel Med Infect Dis. 2019;27:104-6. PubMed PMID: 29751131.
829 39. Love MI, Huber W, Anders S. Moderated estimation of fold change and dispersion for
830 RNA-seq data with DESeq2. Genome Biol. 2014;15(12):550. PubMed PMID: 25516281.

831 40. Bindea G, Mlecnik B, Hackl H, Charoentong P, Tosolini M, Kirilovsky A, Fridman WH,
832 Pages F, Trajanoski Z, Galon J. ClueGO: a Cytoscape plug-in to decipher functionally
833 grouped gene ontology and pathway annotation networks. Bioinformatics. 2009;25(8):1091-
834 3. PubMed PMID: 19237447.
835 41. Mlecnik B, Bindea G, Angell HK, Sasso MS, Obenauf AC, Fredriksen T, Lafontaine L,
836 Bilocq AM, Kirilovsky A, Tosolini M, Waldner M, Berger A, et al. Functional network pipeline
837 reveals genetic determinants associated with in situ lymphocyte proliferation and survival of
838 cancer patients. Sci Transl Med. 2014;6(228):228ra37. PubMed PMID: 24648340.
839 42. Tran TM, Jones MB, Ongoiba A, Bijker EM, Schats R, Venepally P, Skinner J,
840 Doumbo S, Quinten E, Visser LG, Whalen E, Presnell S, et al. Transcriptomic evidence for
841 modulation of host inflammatory responses during febrile Plasmodium falciparum malaria.
842 Sci Rep. 2016;6:31291. PubMed PMID: 27506615.
843 43. Ockenhouse CF, Hu WC, Kester KE, Cummings JF, Stewart A, Heppner DG,
844 Jedlicka AE, Scott AL, Wolfe ND, Vahey M, Burke DS. Common and divergent immune
845 response signaling pathways discovered in peripheral blood mononuclear cell gene
846 expression patterns in presymptomatic and clinically apparent malaria. Infect Immun.
847 2006;74(10):5561-73. PubMed PMID: 16988231.
848 44. Spaulding E, Fooksman D, Moore JM, Saidi A, Feintuch CM, Reizis B, Chorro L,
849 Daily J, Lauvau G. STING-Licensed Macrophages Prime Type I IFN Production by
850 Plasmacytoid Dendritic Cells in the Bone Marrow during Severe Plasmodium yoelii Malaria.
851 PLoS Pathog. 2016;12(10):e1005975. PubMed PMID: 27792766.
852 45. Hviid L, Kurtzhals JA, Goka BQ, Oliver-Commey JO, Nkrumah FK, Theander TG.
853 Rapid reemergence of T cells into peripheral circulation following treatment of severe and
854 uncomplicated Plasmodium falciparum malaria. Infect Immun. 1997;65(10):4090-3. PubMed
855 PMID: 9317012.
856 46. McInnes L, Healy J, Melville J. UMAP: Uniform Manifold Approximation and
857 Projection for Dimension Reduction. arXiv:180203426. 2020.
858 47. Van Gassen S, Callebaut B, Van Helden MJ, Lambrecht BN, Demeester P, Dhaene
859 T, Saeys Y. FlowSOM: Using self-organizing maps for visualization and interpretation of
860 cytometry data. Cytometry A. 2015;87(7):636-45. PubMed PMID: 25573116.
861 48. Robinson MD, McCarthy DJ, Smyth GK. edgeR: a Bioconductor package for
862 differential expression analysis of digital gene expression data. Bioinformatics.
863 2010;26(1):139-40. PubMed PMID: 19910308.
864 49. Weber LM, Nowicka M, Soneson C, Robinson MD. diffcyt: Differential discovery in
865 high-dimensional cytometry via high-resolution clustering. Commun Biol. 2019;2:183.
866 PubMed PMID: 31098416.
867 50. Napolitani G, Kurupati P, Teng KWW, Gibani MM, Rei M, Aulicino A, Preciado-Llanes
868 L, Wong MT, Becht E, Howson L, de Haas P, Salio M, et al. Clonal analysis of Salmonella-
869 specific effector T cells reveals serovar-specific and cross-reactive T cell responses. Nat
870 Immunol. 2018;19(7):742-54. PubMed PMID: 29925993.
871 51. Rahil Z, Leylek R, Schurch CM, Chen H, Bjornson-Hooper Z, Christensen SR,
872 Gherardini PF, Bhate SS, Spitzer MH, Fragiadakis GK, Mukherjee N, Kim N, et al.
873 Landscape of coordinated immune responses to H1N1 challenge in humans. J Clin Invest.
874 2020;130(11):5800-16. PubMed PMID: 33044226.
875 52. Kaminski LC, Riehn M, Abel A, Steeg C, Yar DD, Addai-Mensah O, Aminkiah F,
876 Owusu Dabo E, Jacobs T, Mackroth MS. Cytotoxic T Cell-Derived Granzyme B Is Increased

877 in Severe Plasmodium Falciparum Malaria. Front Immunol. 2019;10:2917. PubMed PMID:
878 31921176.
879 53. Winkler F, Bengsch B. Use of Mass Cytometry to Profile Human T Cell Exhaustion.
880 Front Immunol. 2019;10:3039. PubMed PMID: 32038613.
881 54. Appay V, Zaunders JJ, Papagno L, Sutton J, Jaramillo A, Waters A, Easterbrook P,
882 Grey P, Smith D, McMichael AJ, Cooper DA, Rowland-Jones SL, et al. Characterization of
883 CD4(+) CTLs ex vivo. J Immunol. 2002;168(11):5954-8. PubMed PMID: 12023402.
884 55. Nikitina IY, Kondratuk NA, Kosmiadi GA, Amansahedov RB, Vasilyeva IA, Ganusov
885 VV, Lyadova IV. Mtb-specific CD27low CD4 T cells as markers of lung tissue destruction
886 during pulmonary tuberculosis in humans. PLoS One. 2012;7(8):e43733. PubMed PMID:
887 22937086.
888 56. Mattoo H, Mahajan VS, Maehara T, Deshpande V, Della-Torre E, Wallace ZS,
889 Kulikova M, Drijvers JM, Daccache J, Carruthers MN, Castelino FV, Stone JR, et al. Clonal
890 expansion of CD4(+) cytotoxic T lymphocytes in patients with IgG4-related disease. J Allergy
891 Clin Immunol. 2016;138(3):825-38. PubMed PMID: 26971690.
892 57. Fonseka CY, Rao DA, Teslovich NC, Korsunsky I, Hannes SK, Slowikowski K,
893 Gurish MF, Donlin LT, Lederer JA, Weinblatt ME, Massarotti EM, Coblyn JS, et al. Mixed-
894 effects association of single cells identifies an expanded effector CD4(+) T cell subset in
895 rheumatoid arthritis. Sci Transl Med. 2018;10(463). PubMed PMID: 30333237.
896 58. Kim J, Chang DY, Lee HW, Lee H, Kim JH, Sung PS, Kim KH, Hong SH, Kang W,
897 Lee J, Shin SY, Yu HT, et al. Innate-like Cytotoxic Function of Bystander-Activated CD8(+) T
898 Cells Is Associated with Liver Injury in Acute Hepatitis A. Immunity. 2018;48(1):161-73 e5.
899 PubMed PMID: 29305140.
900 59. Lee HG, Cho MZ, Choi JM. Bystander CD4(+) T cells: crossroads between innate
901 and adaptive immunity. Exp Mol Med. 2020;52(8):1255-63. PubMed PMID: 32859954.
902 60. Raue HP, Beadling C, Haun J, Slifka MK. Cytokine-mediated programmed
903 proliferation of virus-specific CD8(+) memory T cells. Immunity. 2013;38(1):131-9. PubMed
904 PMID: 23260193.
905 61. Ussher JE, Bilton M, Attwod E, Shadwell J, Richardson R, de Lara C, Mettke E,
906 Kurioka A, Hansen TH, Klenerman P, Willberg CB. CD161++ CD8+ T cells, including the
907 MAIT cell subset, are specifically activated by IL-12+IL-18 in a TCR-independent manner.
908 Eur J Immunol. 2014;44(1):195-203. PubMed PMID: 24019201.
909 62. Gupta R, Kim S, Taylor MW. Suppression of ribosomal protein synthesis and protein
910 translation factors by Peg-interferon alpha/ribavirin in HCV patients blood mononuclear cells
911 (PBMC). J Transl Med. 2012;10:54. PubMed PMID: 22436241.
912 63. Furusawa J, Mizoguchi I, Chiba Y, Hisada M, Kobayashi F, Yoshida H, Nakae S,
913 Tsuchida A, Matsumoto T, Ema H, Mizuguchi J, Yoshimoto T. Promotion of Expansion and
914 Differentiation of Hematopoietic Stem Cells by Interleukin-27 into Myeloid Progenitors to
915 Control Infection in Emergency Myelopoiesis. PLoS Pathog. 2016;12(3):e1005507. PubMed
916 PMID: 26991425.
917 64. Bourgard C, Albrecht L, Kayano A, Sunnerhagen P, Costa FTM. Plasmodium vivax
918 Biology: Insights Provided by Genomics, Transcriptomics and Proteomics. Front Cell Infect
919 Microbiol. 2018;8:34. PubMed PMID: 29473024.
920 65. Mueller I, Galinski MR, Baird JK, Carlton JM, Kochar DK, Alonso PL, del Portillo HA.
921 Key gaps in the knowledge of Plasmodium vivax, a neglected human malaria parasite.
922 Lancet Infect Dis. 2009;9(9):555-66. PubMed PMID: 19695492.

923 66. Nahrendorf W, Ivens A, Spence PJ. Inducible mechanisms of disease tolerance
924 provide an alternative strategy of acquired immunity to malaria. bioRxiv
925 (doi:101101/20201001322180). 2020.
926 67. McKenzie FE, Jeffery GM, Collins WE. Plasmodium vivax blood-stage dynamics. J
927 Parasitol. 2002;88(3):521-35. PubMed PMID: 12099421.
928 68. Wassmer SC, Taylor TE, Rathod PK, Mishra SK, Mohanty S, Arevalo-Herrera M,
929 Duraisingh MT, Smith JD. Investigating the Pathogenesis of Severe Malaria: A
930 Multidisciplinary and Cross-Geographical Approach. Am J Trop Med Hyg. 2015;93(3
931 Suppl):42-56. PubMed PMID: 26259939.
932 69. Dunst J, Kamena F, Matuschewski K. Cytokines and Chemokines in Cerebral
933 Malaria Pathogenesis. Front Cell Infect Microbiol. 2017;7:324. PubMed PMID: 28775960.
934 70. Kjer-Nielsen L, Patel O, Corbett AJ, Le Nours J, Meehan B, Liu L, Bhati M, Chen Z,
935 Kostenko L, Reantragoon R, Williamson NA, Purcell AW, et al. MR1 presents microbial
936 vitamin B metabolites to MAIT cells. Nature. 2012;491(7426):717-23. PubMed PMID:
937 23051753.
938 71. Chua WJ, Truscott SM, Eickhoff CS, Blazevic A, Hoft DF, Hansen TH. Polyclonal
939 mucosa-associated invariant T cells have unique innate functions in bacterial infection. Infect
940 Immun. 2012;80(9):3256-67. PubMed PMID: 22778103.
941 72. Sakala IG, Kjer-Nielsen L, Eickhoff CS, Wang X, Blazevic A, Liu L, Fairlie DP,
942 Rossjohn J, McCluskey J, Fremont DH, Hansen TH, Hoft DF. Functional Heterogeneity and
943 Antimycobacterial Effects of Mouse Mucosal-Associated Invariant T Cells Specific for
944 Riboflavin Metabolites. J Immunol. 2015;195(2):587-601. PubMed PMID: 26063000.
945 73. Hu B, Ren J, Luo Y, Keith B, Young RM, Scholler J, Zhao Y, June CH. Augmentation
946 of Antitumor Immunity by Human and Mouse CAR T Cells Secreting IL-18. Cell Rep.
947 2017;20(13):3025-33. PubMed PMID: 28954221.
948 74. Smith NL, Nahrendorf W, Sutherland C, Mooney JP, Thompson J, Spence PJ,
949 Cowan GJM. A Conserved TCRbeta Signature Dominates a Highly Polyclonal T-Cell
950 Expansion During the Acute Phase of a Murine Malaria Infection. Front Immunol.
951 2020;11:587756. PubMed PMID: 33329568.
952 75. Weng NP, Liu K, Catalfamo M, Li Y, Henkart PA. IL-15 is a growth factor and an
953 activator of CD8 memory T cells. Ann N Y Acad Sci. 2002;975:46-56. PubMed PMID:
954 12538153.
955 76. Sallusto F, Cassotta A, Hoces D, Foglierini M, Lanzavecchia A. Do Memory CD4 T
956 Cells Keep Their Cell-Type Programming: Plasticity versus Fate Commitment? T-Cell
957 Heterogeneity, Plasticity, and Selection in Humans. Cold Spring Harb Perspect Biol.
958 2018;10(3). PubMed PMID: 28432133.
959 77. Brodin P, Davis MM. Human immune system variation. Nat Rev Immunol.
960 2017;17(1):21-9. PubMed PMID: 27916977.
961 78. Tsang JS, Schwartzberg PL, Kotliarov Y, Biancotto A, Xie Z, Germain RN, Wang E,
962 Olnes MJ, Narayanan M, Golding H, Moir S, Dickler HB, et al. Global analyses of human
963 immune variation reveal baseline predictors of postvaccination responses. Cell.
964 2014;157(2):499-513. PubMed PMID: 24725414.
965 79. Hou L, Huang H. Immune suppressive properties of artemisinin family drugs.
966 Pharmacol Ther. 2016;166:123-7. PubMed PMID: 27411673.

967 80. Wang JX, Tang W, Shi LP, Wan J, Zhou R, Ni J, Fu YF, Yang YF, Li Y, Zuo JP.
968 Investigation of the immunosuppressive activity of artemether on T-cell activation and
969 proliferation. Br J Pharmacol. 2007;150(5):652-61. PubMed PMID: 17262016.
970 81. Andrade BB, Reis-Filho A, Souza-Neto SM, Clarencio J, Camargo LM, Barral A,
971 Barral-Netto M. Severe Plasmodium vivax malaria exhibits marked inflammatory imbalance.
972 Malar J. 2010;9:13. PubMed PMID: 20070895.
973 82. Apte SH, Minigo G, Groves PL, Spargo JC, Plebanski M, Grigg MJ, Kenangalem E,
974 Burel JG, Loughland JR, Flanagan KL, Piera KA, William T, et al. A population of
975 CD4(hi)CD38(hi) T cells correlates with disease severity in patients with acute malaria. Clin
976 Transl Immunology. 2020;9(11):e1209. PubMed PMID: 33282291.
977 83. Gatton ML, Cheng Q. Evaluation of the pyrogenic threshold for Plasmodium
978 falciparum malaria in naive individuals. Am J Trop Med Hyg. 2002;66(5):467-73. PubMed
979 PMID: 12201578.
980 84. Goncalves BP, Huang CY, Morrison R, Holte S, Kabyemela E, Prevots DR, Fried M,
981 Duffy PE. Parasite burden and severity of malaria in Tanzanian children. N Engl J Med.
982 2014;370(19):1799-808. PubMed PMID: 24806160.
983 85. Glynn JR, Collins WE, Jeffery GM, Bradley DJ. Infecting dose and severity of
984 falciparum malaria. Trans R Soc Trop Med Hyg. 1995;89(3):281-3. PubMed PMID: 7660433.
985 86. Gu Z, Eils R, Schlesner M. Complex heatmaps reveal patterns and correlations in
986 multidimensional genomic data. Bioinformatics. 2016;32(18):2847-9. PubMed PMID:
987 27207943.
988 87. Crowell H, Zanotelli V, Chevrier S, Robinson M. CATALYST: Cytometry dATa
989 anALYSis Tools. R/Bioconductor. 2020;version 1.14.0.
990 88. Wickam H. ggplot2: Elegant Graphics for Data Analysis. Springer-Verlag New York.
991 2016.
992 89. Langmead B, Salzberg SL. Fast gapped-read alignment with Bowtie 2. Nat Methods.
993 2012;9(4):357-9. PubMed PMID: 22388286.
994 90. Finck R, Simonds EF, Jager A, Krishnaswamy S, Sachs K, Fantl W, Pe'er D, Nolan
995 GP, Bendall SC. Normalization of mass cytometry data with bead standards. Cytometry A.
996 2013;83(5):483-94. PubMed PMID: 23512433.
997 91. Zunder ER, Finck R, Behbehani GK, Amir el AD, Krishnaswamy S, Gonzalez VD,
998 Lorang CG, Bjornson Z, Spitzer MH, Bodenmiller B, Fantl WJ, Pe'er D, et al. Palladium-
999 based mass tag cell barcoding with a doublet-filtering scheme and single-cell deconvolution
1000 algorithm. Nat Protoc. 2015;10(2):316-33. PubMed PMID: 25612231.
1001 92. Nowicka M, Krieg C, Crowell HL, Weber LM, Hartmann FJ, Guglietta S, Becher B,
1002 Levesque MP, Robinson MD. CyTOF workflow: differential discovery in high-throughput
1003 high-dimensional cytometry datasets. F1000Res. 2017;6:748. PubMed PMID: 28663787.
1004 93. Chevrier S, Crowell HL, Zanotelli VRT, Engler S, Robinson MD, Bodenmiller B.
1005 Compensation of Signal Spillover in Suspension and Imaging Mass Cytometry. Cell Syst.
1006 2018;6(5):612-20 e5. PubMed PMID: 29605184.
1007 94. McCarthy DJ, Campbell KR, Lun AT, Wills QF. Scater: pre-processing, quality
1008 control, normalization and visualization of single-cell RNA-seq data in R. Bioinformatics.
1009 2017;33(8):1179-86. PubMed PMID: 28088763.
1010 95. Saeys Y, Van Gassen S, Lambrecht B. Response to Orlova et al. "Science not art:
1011 statistically sound methods for identifying subsets in multi-dimensional flow and mass
1012 cytometry data sets". Nat Rev Immunol. 2017;18(1):78. PubMed PMID: 29269765.

1013 96. Payne RO, Milne KH, Elias SC, Edwards NJ, Douglas AD, Brown RE, Silk SE,
1014 Biswas S, Miura K, Roberts R, Rampling TW, Venkatraman N, et al. Demonstration of the
1015 Blood-Stage Plasmodium falciparum Controlled Human Malaria Infection Model to Assess
1016 Efficacy of the P. falciparum Apical Membrane Antigen 1 Vaccine, FMP2.1/AS01. J Infect
1017 Dis. 2016;213(11):1743-51. PubMed PMID: 26908756.